

Key Points:

- Large increases (~10–30%) in summer hypoxic and anoxic volumes are projected for the mid-21st century
- Decreasing physical supply of oxygen is offset by reduced summer respiration
- Decreasing O₂ solubility accounts for about 50% of the total projected oxygen decline

Correspondence to:

W. Ni,
wni@umces.edu

Citation:

Ni, W., Li, M., Ross, A. C., & Najjar, R. G. (2019). Large projected decline in dissolved oxygen in a eutrophic estuary due to climate change. *Journal of Geophysical Research: Oceans*, 124, 8271–8289. <https://doi.org/10.1029/2019JC015274>

Received 9 MAY 2019

Accepted 10 NOV 2019

Accepted article online 22 NOV 2019

Published online 25 NOV 2019

Large Projected Decline in Dissolved Oxygen in a Eutrophic Estuary Due to Climate Change

Wenfei Ni¹ , Ming Li¹ , Andrew C. Ross^{2,3} , and Raymond G. Najjar³ 

¹Horn Point Laboratory, University of Maryland Center for Environmental Science, Cambridge, MD, USA, ²Princeton University Program in Atmospheric and Oceanic Sciences and NOAA Geophysical Fluid Dynamics Laboratory, Princeton, NJ, USA, ³Department of Meteorology and Atmospheric Science, Pennsylvania State University, University Park, PA, USA

Abstract Climate change is known to cause deoxygenation in the open ocean, but its effects on eutrophic and seasonally hypoxic estuaries and coastal oceans are less clear. Using Chesapeake Bay as a study site, we conducted climate downscaling projections for dissolved oxygen and found that the hypoxic and anoxic volumes would increase by 10–30% between the late 20th and mid-21st century. A budget analysis of dissolved oxygen in the bottom water revealed differing physical and biogeochemical responses to climate change. Sea level rise and larger winter-spring runoff led to stronger stratification and large reductions in the vertical oxygen supply to the bottom water. On the other hand, warming led to earlier initiation of hypoxia, accompanied by weaker summer respiration and more rapid termination of hypoxia. Decreasing solubility due to warming accounted for about 50% of the reduction in the bottom-water oxygen content.

1. Introduction

Dissolved oxygen (O₂) concentration has been declining in both the open ocean and coastal waters (Breitburg et al., 2018; Diaz & Rosenberg, 2008). In the open ocean, the oxygen loss is primarily linked to global warming and other climate change effects (Levin, 2018; Schmidtke et al., 2017; Stramma et al., 2008). Among the most relevant deoxygenation drivers, warming reduces ventilation of deeper waters due to stronger stratification in the upper ocean and decreases oxygen solubility (Keeling et al., 2010) while raising microbial metabolic rates and oxygen consumption (Deutsch et al., 2011). In estuaries and coastal oceans, the depletion of oxygen in bottom water has occurred at faster rates than the open ocean (Gilbert et al., 2010) and has been traditionally attributed to nutrient and organic matter loading from the surrounding watershed and rivers (Fennel & Testa, 2019; Kemp et al., 2009; Rabalais et al., 2014). Nevertheless, there is increasing recognition that climate change can also significantly affect hypoxia in estuarine and coastal waters (Altieri & Gedan, 2015; Bendtsen & Hansen, 2013; Claret et al., 2018; Justic et al., 2003; Meier et al., 2011).

Climate change and climate variability can affect physical processes regulating the supply of O₂ to the bottom water. In coastal and estuarine waters, freshwater input sustains the stratification that contributes to the formation of summer oxygen depletion. As a consequence, variations in the hydrologic cycle can affect the extent of hypoxia from interannual to long-term time scales (Du et al., 2018; Yu et al., 2015; Zillén et al., 2008). Wind affects O₂ by regulating mixing and advection of O₂ to the bottom water (Feng et al., 2012; Scully, 2013, 2016a; Wilson et al., 2008). Climate change and climate variability can also affect biogeochemical processes that consume O₂ in the water column and sediment. Nutrient loading from river runoff was shown to drive interannual hypoxia variations by regulating phytoplankton growth and water column respiration (Justic et al., 2002; Li et al., 2016). Similarly, Große et al. (2016) found that biological production is a major driver of oxygen deficiency in some parts of the North Sea.

With climate change projected to accelerate in the 21st century, it is important to take into consideration its effects when modeling hypoxia in estuarine and coastal waters and developing nutrient management strategies (Breitburg et al., 2018). Using an ensemble of coupled physical-biogeochemical models driven by regionalized global climate model (GCM) outputs, Meier et al. (2011) projected that the hypoxic and anoxic areas in the Baltic Sea will increase in the future climate. This regional deoxygenation is caused by reduced oxygen solubility and intensified internal nutrient cycling, both of which result from increased temperature. Model simulations also showed that the warming induced decline of oxygen solubility and intensified

stratification will lead to significant decrease of bottom-water O₂ in the North Sea and Gulf of Mexico by the end of 21st century (Laurent et al., 2018; Meire et al., 2013). In a recent modeling study, however, Saraiva et al. (2019a) found that the effects of climate change are smaller than the effects of considered nutrient load changes in the Baltic Sea.

Chesapeake Bay, the largest estuary in the United States, is characterized by high biological productivity and abundant fishery resources. It is a partially mixed estuary with a deep central channel where summer hypoxia mostly occurs. Hypoxia in Chesapeake Bay experienced dramatic expansion due to nutrient enrichment between the 1950s and 1980s but has stabilized since the mid-1990s (Hagy et al., 2004). Water column oxygen consumption accounts for most of the oxygen demand and drives the interannual variations of hypoxia in the bay (Kemp et al., 1997; Li et al., 2016). Freshwater discharge sustains the stratification that contributes to the formation of summer low-oxygen water (Scully, 2016b; Zhou et al., 2014). Chesapeake Bay has experienced rapid climate change in recent decades, including rapid warming and accelerating relative sea level rise (Boon & Mitchell, 2015; Ding & Elmore, 2015). Therefore, there is increasing recognition and concern about climate change impacts on Chesapeake Bay (Najjar et al., 2010).

Two recent modeling studies have examined the impacts of climate change on hypoxia in Chesapeake Bay, but they were forced by simplified changes from climate model projections. Wang et al. (2017) investigated the individual and combined effects of warming and sea level rise by 2050. Summer anoxic volume was estimated to increase by 1.4% due to warming, but sea level rise resulted in a 12% reduction in the anoxic volume. In addition to warming and sea level rise, Irby et al. (2018) considered the effects of altered river flows. They found that warming reduced oxygen solubility year around, changes in precipitation and river flow fueled increased primary production, and sea level rise increased bottom-water O₂ but decreased O₂ at mid-depths. Irby et al. (2018) found that the overall impact of climate change will be to lower O₂ in Chesapeake Bay, but its potential impact is significantly smaller than the improvement in O₂ due to planned nutrient reductions.

The Baltic Sea studies of Meier et al. (2011) and Saraiva et al. (2019b) presented results from ensemble simulations to account for climate uncertainty. This multimodel projection would generate probabilistic and practical impact assessment. However, this approach has not yet been implemented in Chesapeake Bay; previous studies were only based on sensitivity analyses to individual climate change factors or their combined effects (Irby et al., 2018; Wang et al., 2017). They cannot be directly used to make projections for estuarine hypoxia for the future climate. The natural climate variability and connections within the climate system (e.g., the relationship between temperature, precipitation/evapotranspiration, and river discharge change) were also missing in their studies. Therefore, this study utilizes multiple bias-corrected climate projections from high-resolution regional climate models (RCMs) to drive a coupled physical-biogeochemical model and assess the impacts of future climate change on Chesapeake Bay hypoxia. As a large eutrophic estuary with a long history of seasonal hypoxia, Chesapeake Bay is well suited as a representative study site, and the climate downscaling modeling approach developed here is applicable to other estuaries and coastal oceans.

2. Method

To project future changes in Chesapeake Bay hypoxia, we used a coupled physical-biogeochemical model that was shown to be skillful in hindcast simulations (Li et al., 2016; Testa et al., 2014) and forced it primarily with downscaled climate projections from the North American Regional Climate Change Assessment Program (NARCCAP; Mearns et al., 2007). NARCCAP uses a dynamic climate downscaling approach by embedding fine-resolution (about 50 km) RCMs of North America into GCMs from the Coupled Model Intercomparison Project Phase 3 (CMIP3; Figures 1a and 1b and Table 1). Simulations are available for a historical period (1971–2000) and the mid-21st century (2041–2070) under the medium-high A2 greenhouse gas emissions scenario (Nakićenović et al., 2000). Although GCMs results from CMIP5 (Phase 5) are now available, some high-resolution RCMs outputs needed for driving the estuarine model are not yet available (Giorgi & Gutowski, 2015).

The Chesapeake Bay model consists of two submodels. The physical model, based on the Regional Ocean Modeling System (ROMS, Shchepetkin & McWilliams, 2005; Haidvogel et al., 2008), has 82 × 122 grid

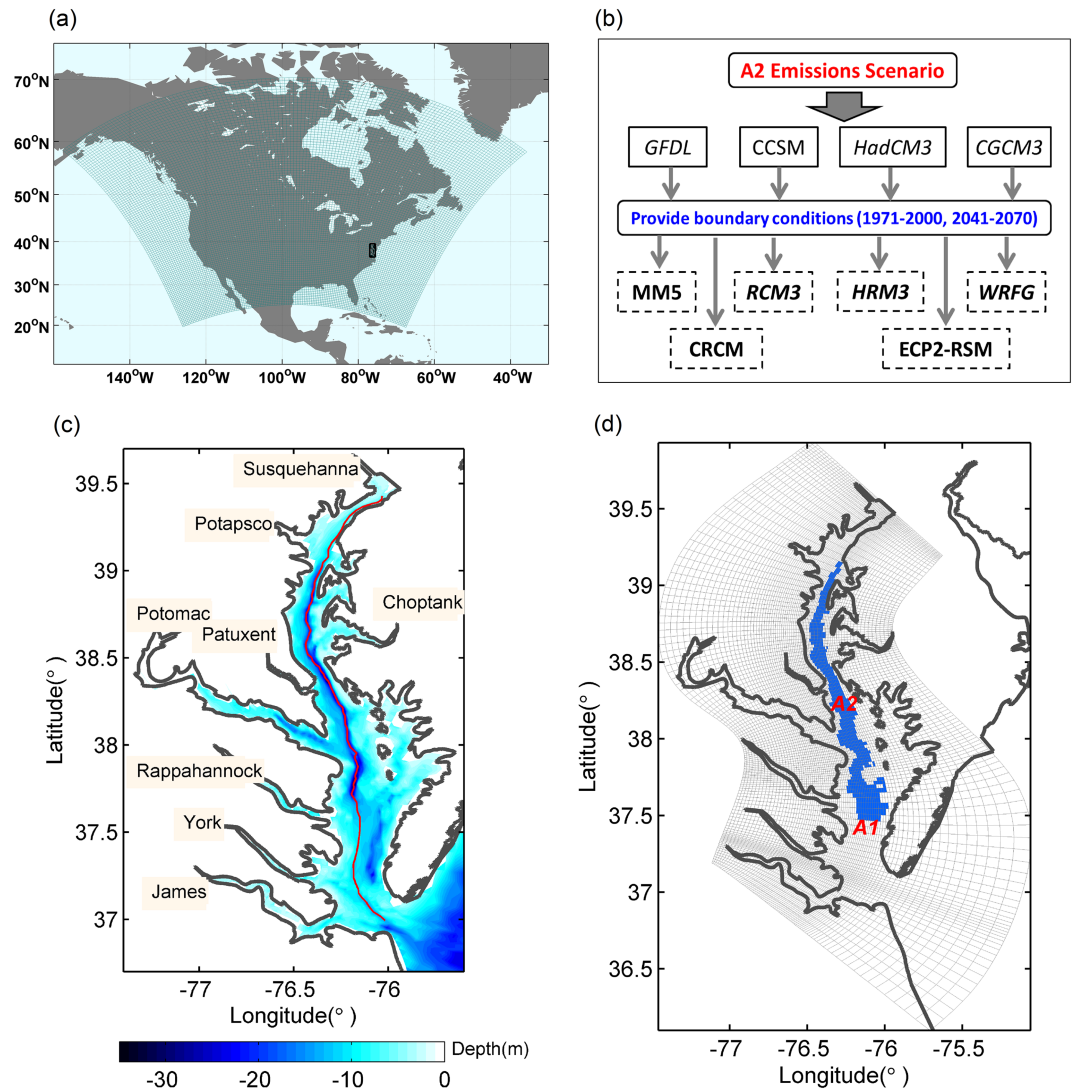


Figure 1. (a) NARCCAP Regional Climate Model domain in North America. The black box indicates the location of Chesapeake Bay. (b) NARCCAP modeling framework, including global climate models (in rectangles with solid line) and regional climate models (bold font, in rectangles with dashed line). The model names in italics indicate the model used in this study. The full model names and references are listed in Table 1. (c) Chesapeake Bay bathymetry. The solid red line marks the along-channel section used to plot the O_2 distributions in Figure 4. (d) The grid for the ROMS-RCA model. The blue area marks the control volume used in oxygen budget analysis in Figures 7 and 11.

points (~1-km resolution) in the horizontal direction and 20 vertical layers with the maximum depth of 40 m in the deep channel (Figures 1c and 1d, Li et al., 2005). ROMS is forced by daily river flows at eight major tributaries, by wind stress and heat fluxes at the sea surface, and by sea level and climatologies of temperature and salinity at the open boundary. At the offshore boundary, the sea level consists of tidal and nontidal forcing (Egbert & Erofeeva, 2002; Li et al., 2005; Table 2). RCM projections for meteorological variables are at 3-hourly intervals and include surface air pressure, relative humidity and air temperature at 2 m above the surface, downwelling longwave radiation and net shortwave radiation at surface, and wind speed at 10 m above the surface. These variables were used to calculate the air-sea fluxes of momentum and heat using the standard bulk formulae (Fairall et al., 2003). To correct the biases in the NARCCAP meteorological outputs, we applied the empirical quantile mapping method, using historical data from the North American Regional Reanalysis as the observational reference (Gudmundsson et al., 2012; Mesinger et al., 2006; Wood et al., 2004). The cumulative distribution functions and quantile functions were constructed separately for each calendar season (December–

Table 1
RCMs and GCMs in NARCCAP (From Mearns et al., 2012)

	Abbr.	Full name	Reference
RCM	CRCM	Canadian Regional Climate Model	Caya & Laprise, 1999
	MM5	The Fifth generation Pennsylvania State University–National Center for Atmospheric Research (NCAR) Mesoscale Model	Grell et al., 1993
	HRM3	The Met Office Hadley Centre's regional climate model version 3	Jones et al., 2003
	RCM3	Regional Climate Model version 3	Giorgi, Marinucci, & Bates, 1993; Giorgi, Marinucci, Bates, & De Canio, 1993; Pal et al., 2000, 2007
	ECP2	Scripps Experimental Climate Prediction Center Regional Spectral Model	Juang et al., 1997
GCM	WRFG	Weather Research and Forecasting model	Skamarock et al., 2005
	CCSM3	NCAR Community Climate System Model, version 3	Collins et al., 2006
	CGCM3	Canadian Climate Centre Coupled General Circulation Model version 3	Scinocca & McFarlane, 2004; Flato, 2005
	HadCM3	The Met Office Hadley Centre's climate model version 3	Gordon et al., 2000; Pope et al., 2000
	GFDL	Geophysical Fluid Dynamics Laboratory Climate Model version 2.1	GFDL Global Atmospheric Model Development Team, 2004

February, March–May, June–August, September–November) for the historical period. For wind, the bias correction was only made on the wind speed magnitude due to larger uncertainty in the climate model projections for wind direction (Morrison et al., 2014) and the univariate nature of the quantile mapping method.

The biogeochemical model is based on the Row-Column Aesop (RCA) model, which consists of a water column component (Isleib et al., 2007) and a sediment diagenesis component (Brady et al., 2013; Di Toro, 2001; Testa et al., 2013). RCA includes two phytoplankton groups, particulate and dissolved forms of organic carbon and nutrients (nitrogen, phosphorus, and silicon), and O₂. The sediment model, which exchanges materials with the water column model, has one aerobic layer and one anaerobic layer and simulates the cycling of carbon, O₂, nitrogen, phosphorus, and sulfur. The RCA model for Chesapeake Bay is described in detail in Testa et al. (2014). To simulate the historical period as a baseline to make future projections, the river inputs of phytoplankton, particulate and dissolved organic carbon, and organic and inorganic nutrients were obtained from Chesapeake Bay Program biweekly monitoring data (<https://www.chesapeakebay.net/what/data>) at eight major tributaries. The ocean boundary inputs were acquired from the World Ocean Atlas 2013 and Filippino et al. (2011; Table 2). Atmospheric deposition was not considered in this study.

To simulate the mid-21st century, GCM projections for the Northwest Atlantic Ocean were used to prescribe changes in the offshore boundary condition for ROMS-RCA. The relative sea level rise was set to be the sum of the CMIP3 sea level projection for the region (Mitrovica et al., 2009; Mitrovica et al., 2011; Slangen et al.,

Table 2
Model Forcing in the Historical and Future Simulations

Boundary		Historical period (1989–1998)	Future period (2049–2058)
Atmosphere		NARCCAP regional climate model outputs with bias correction in 1989–1998	NARCCAP regional climate model outputs with bias correction in 2049–2058
Ocean	Sea level	Tide (TPX07) + non-Tide (Duck) in 1989–1998	Based on historical sea level, add projected sea level change due to thermal expansion, regional dynamics, land glaciers and ice sheet and regional vertical movement
	Salinity	WOA monthly data with decadal average	Same as historical
	Temperature	WOA monthly data with decadal average	Based on historical, add monthly ocean water temperature change projected by GCMs of NARCCAP
	Nutrient	WOA monthly data with decadal average, reference values based on Filippino et al. (2011)	Same as historical
River	Discharge	USGS monitoring daily discharge in 1989–1998	Based on historical, multiply by the monthly scaling factor from NARCCAP model projection on runoff
	Temperature	CBP biweekly measurement in 1989–1998	Based on historical, add future temperature increases assuming at the same rate as Rice and Jastram (2015) for 1961–2010
	Nutrient	CBP biweekly measurement in 1989–1998	Same as historical

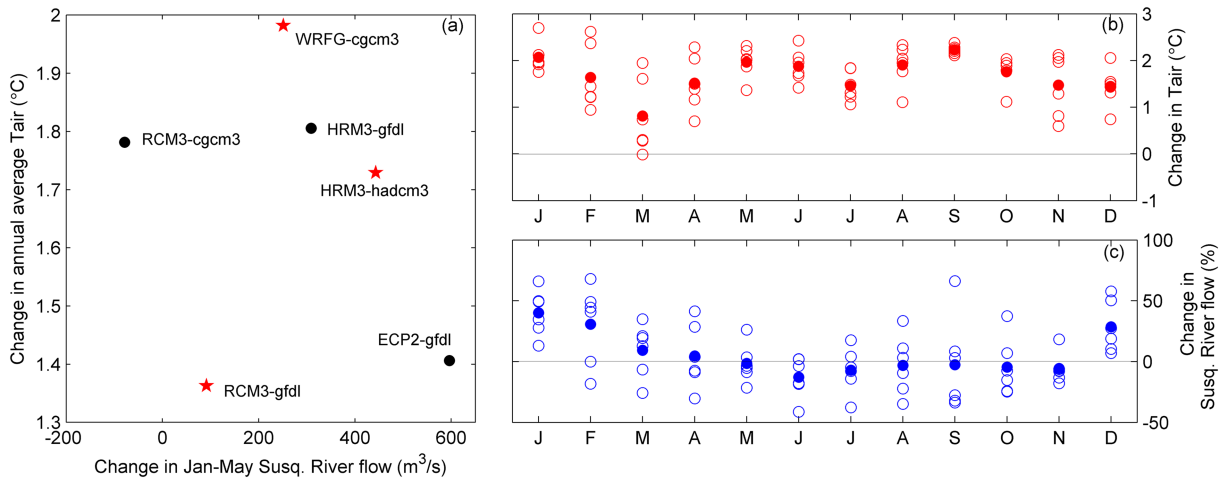


Figure 2. (a) Projected change in the annual mean air temperature (at 2 m above the surface) over Chesapeake Bay versus projected change in Jan–May average Susquehanna River discharge between the late 20th and mid-21st century, obtained from six GCM-RCM models in the NARCCAP ensemble. GCMs are labeled with lowercase letters, and RCMs are labeled with capital letters. The full model names and references are listed in Table 1. The red stars mark three GCM-RCMs used for the hypoxia projections. Scatter plots of projected changes in monthly mean air temperature (b) and monthly mean Susquehanna River flow (c). In (b) and (c), open circles indicate the value of each model in (a); solid circles indicate the ensemble mean.

2012) and the local sea level rise due to land subsidence (Miller et al., 2013; Zervas, 2009), following Boesch et al. (2013) and Lee et al. (2017; Table 2). To set the temperature condition, we calculated the difference of monthly mean water temperature between 1971–2000 and 2041–2070 from the GCM outputs and added this difference to the historical climatology (Table 2). The GCM resolution mostly ranges from 1° to 2° in latitude and 2° to 4° in longitude which is too coarse to fully resolve nearshore physical and biological processes (Chapman & Beardsley, 1989; Fennel et al., 2006). One process is the northward shift of the Gulf Stream which may influence the hydrography and biogeochemistry of Chesapeake Bay (Saba et al., 2016). In this study the salinity and nutrient concentrations were assumed to remain the same at the offshore boundary (Table 2).

RCMs in NARCCAP include basic land-surface schemes that interact with the atmosphere to generate surface runoff (Milly & Dunne, 2011), but they do not include hydrological models or river routing models that can simulate streamflow. Here we assumed that future changes in river discharge Q can be approximated by changes in the integrated runoff R over the watershed (Table 2). Climate-induced changes in riverine nutrient and organic matter loading were assumed to be caused by changes in the river flows only. Potential impacts of nutrient management strategies (Linker et al., 2013) and climate-induced changes in watershed denitrification (Howarth et al., 2006; Schaefer & Alber, 2007) were not considered.

There are a total of 12 RCM-GCM combinations in NARCCAP (Table 1, Mearns et al., 2012, 2013). Six of these combinations have a complete data set available over Chesapeake Bay and its watershed. The projected changes in surface air temperature over Chesapeake Bay and the winter-spring Susquehanna River flow between the late 20th and mid-21st century are shown in Figure 2. All six models predict substantial increases in the annual mean air temperature, with the ensemble mean of about 1.68 °C and a range from 1.35 to 1.95 °C (Figure 2a). The January–May Susquehanna River flow shows increases in five models, ranging from a low of 92 m³ s⁻¹ in RCM3_gfdl to a high of 600 m³ s⁻¹ in ECP2_gfdl (Figure 2a). Figures 2b and 2c show the projected changes in monthly mean surface air temperature and monthly mean Susquehanna River flow among the models. There are substantial seasonal variations in the changes of temperature and river flow between the late 20th and mid-21st century. Warming in air during the summer is greatest and has smaller intermodel differences than other seasons (Figure 2b). The river flow is projected to increase up to 40% during the winter months (December–February; Figure 2c). The spring flow is also projected to increase, but there are large uncertainties among the models. Most models predict a moderate decrease in river flow in summer, with a 5–10% decline in the model ensemble mean.

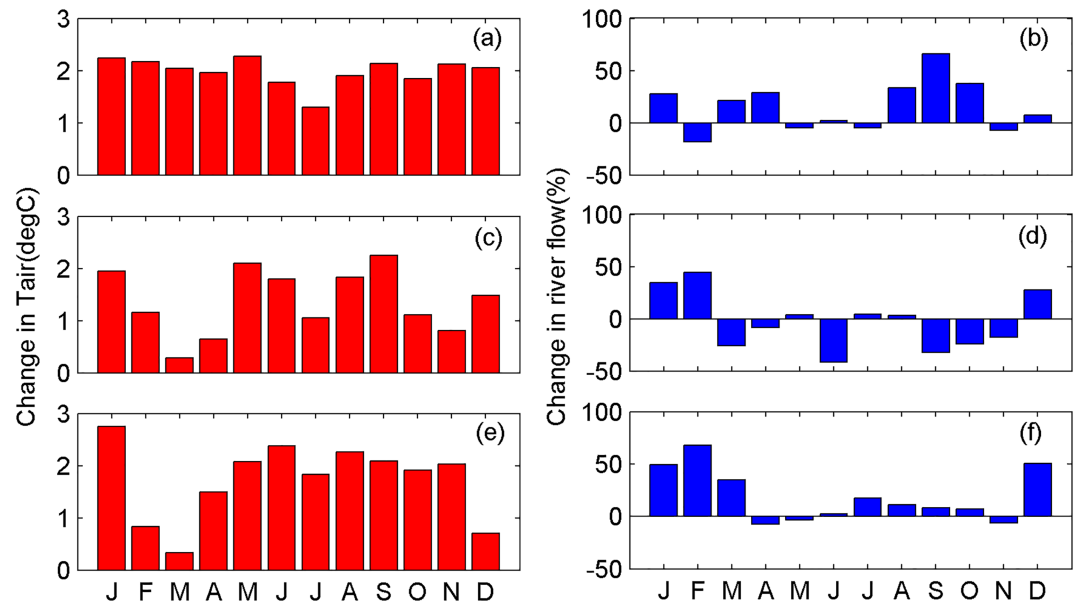


Figure 3. Projected changes in surface air temperature over Chesapeake Bay (left column) and Susquehanna River discharge (right column) between the late 20th century and mid-21st century, obtained from WRFG_cgcm3 (a, b), RCM3_gfdl (c, d), and HRM3_hadcm3 (e, f).

For the climate downscaling projections for Chesapeake Bay hypoxia, we selected RCM3_gfdl, HRM3_hadcm3, and WRFG_cgcm3 which capture the spreads among the NARCCAP ensemble members (Figure 2a). RCM3_gfdl is the Regional Climate Model version 3 (RCM3, Pal et al., 2007) driven by the Geophysical Fluid Dynamics Laboratory model (GFDL, Delworth et al., 2006), projecting relatively low temperature and streamflow changes. HRM3_hadcm3 is the Hadley Regional Climate Model (HRM3, Jones et al., 2003) driven by the Hadley Centre Coupled Model version 3 (HadCM3, Gordon et al., 2000), projecting moderate temperature increase but large streamflow increase. WRFG_cgcm3 is the Weather Research and Forecasting Grell model (WRFG; Skamarock et al., 2005) driven by the Third Generation Coupled Global Climate Model (CGCM3; Flato, 2005), projecting large temperature increase but moderate streamflow increase. Figure 3 shows the projected monthly changes in air temperature and the Susquehanna River flow from the three RCMs. WRFG_cgcm3 projects large temperature increases (about 1.9 °C) with weak seasonal variations. It also predicts the river flow to increase in winter and spring, decrease slightly in summer, and increase substantially in the fall. RCM3_gfdl predicts smaller warming (about 1.4 °C) with strong seasonal variations. It also projects an increase in the winter river discharge but mostly decreases in other seasons. HRM3_hadcm3 predicts moderate increases in temperature (about 1.7 °C) but with strong seasonal variations and large increases in winter river flows but small changes of either sign during other seasons. These three GCM-RCM combinations are not only representative of the ensemble mean projection but also capture the spreads within the NACCARP ensemble.

Hypoxia in Chesapeake Bay experienced dramatic expansion due to eutrophication between the 1950s and 1980s but has stabilized since the mid-1990s (Hagy et al., 2004). We chose 10 years (1989–1998) in the late 20th century within the NARCCAP historical period to conduct ROMS-RCA reference simulations. ROMS-RCA future simulations were conducted for 10 years (2049–2058) in the mid-21st century. The ROMS hydrodynamic model was spun up for 2 years to reach a quasi steady state and then run continuously for the late 20th century (1989–1998) and mid-21st century (2049–2058) simulations, respectively. The initial condition of the RCA biogeochemical model was based on Chesapeake Bay Program monitoring data for the historical period but adjusted to include the effects of warming on decreasing oxygen solubility in the mid-21st century. Specifically, oxygen saturation concentration is calculated using temperature and salinity from the historical and future ROMS model runs. Adding the difference in the oxygen saturation concentration to the initial O₂ condition in the historical RCA run then sets the initial condition for the future RCA run.

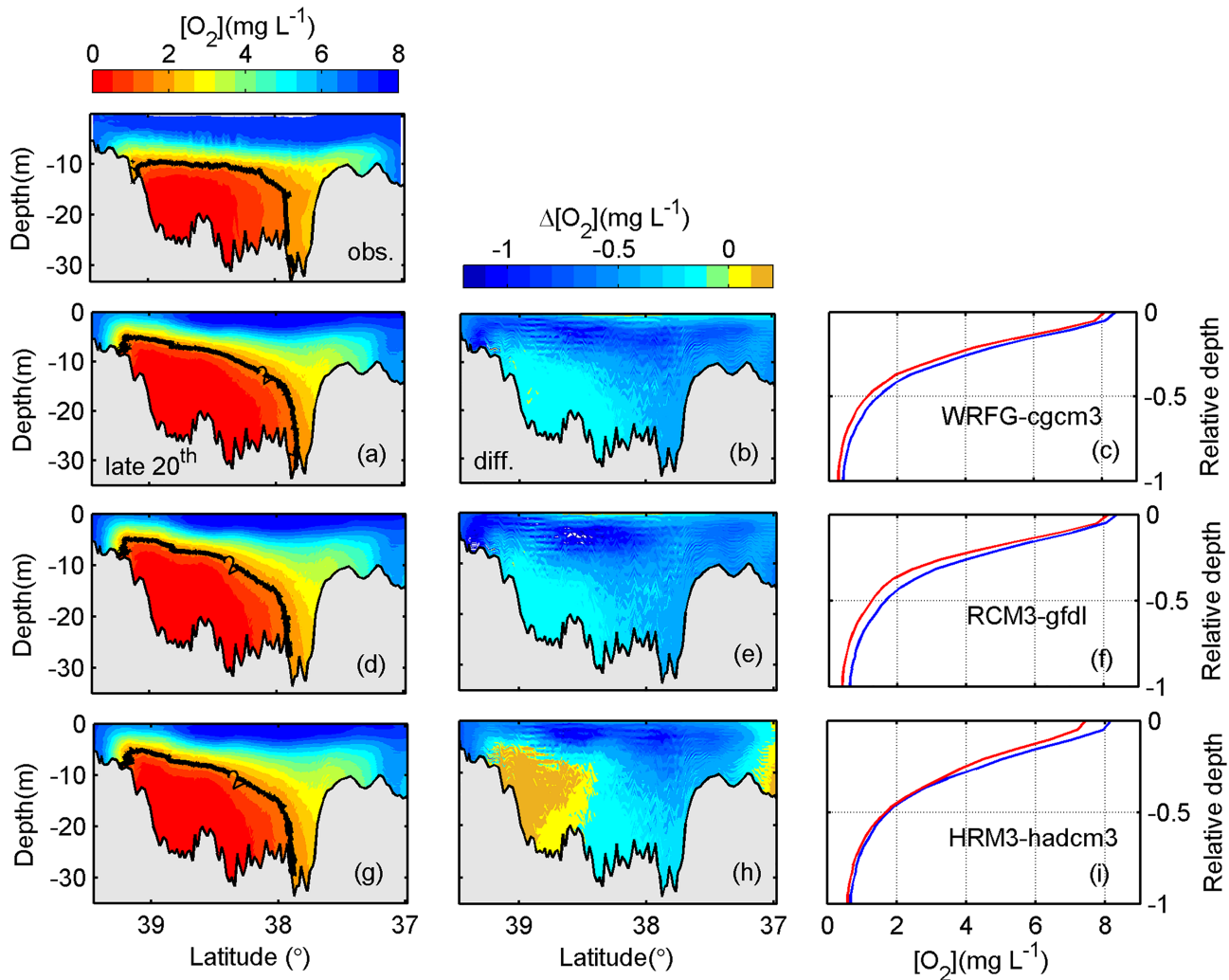


Figure 4. Observed (top panel) and (a, d, g) simulated climatological mean distribution of the summer O_2 concentration along the center deep channel of Chesapeake Bay in the late 20th century. The thick black line is the $O_2 = 2 \text{ mg L}^{-1}$ contour which defines the threshold oxygen concentration for hypoxia. (b, e, h) O_2 changes between the late 20th and mid-21st century. (c, f, i) Vertical profiles of the mean oxygen concentration of the deep water region ($>20 \text{ m}$) of Chesapeake Bay in the late 20th century (blue) and the mid-21st century (red) plotted versus the relative depth, which is defined as the depth of a layer divided by the total water depth. The RCMs are WRFG_cgcm3 (a–c), RCM3_gfdl (d–f), and HRM3_hadcm3 (g–i).

3. Results

3.1. Simulated O_2 Change

To show O_2 changes between the late 20th and mid-21st century, we calculated the climatological mean (10-year average) O_2 concentration for the summer months (June–August) and plotted its distribution along the center deep channel (its location marked in Figure 1c). For comparison, observed O_2 at a number of monitoring stations managed by Chesapeake Bay Program (<https://www.chesapeakebay.net>) were interpolated onto the model grids along the deep channel of the estuary (Figure 4, obs). ROMS-RCA produced realistic simulations of the observed O_2 distribution in 1989–1998: The hypoxic water occupies the deep channel in the mid-Bay (Figures 4a, 4d, and 4g). The Taylor diagram (Taylor, 2001) provides a quantitative evaluation of the model's skill in predicting the time series of the surface and bottom O_2 at a mid-Bay monitoring station (CB 4.3C) as well the time series of the hypoxic ($O_2 < 2 \text{ mg L}^{-1}$) and anoxic ($O_2 < 0.2 \text{ mg L}^{-1}$) volumes in the Bay (Figure 5). These thresholds of hypoxia and anoxia are chosen according to hypoxia-related ecological effects (Hagy et al., 2004). The correlation coefficient varies from 0.90 to 0.95, indicating that ROMS-RCA accurately captures the phase information in the O_2 time series. The normalized standard deviation

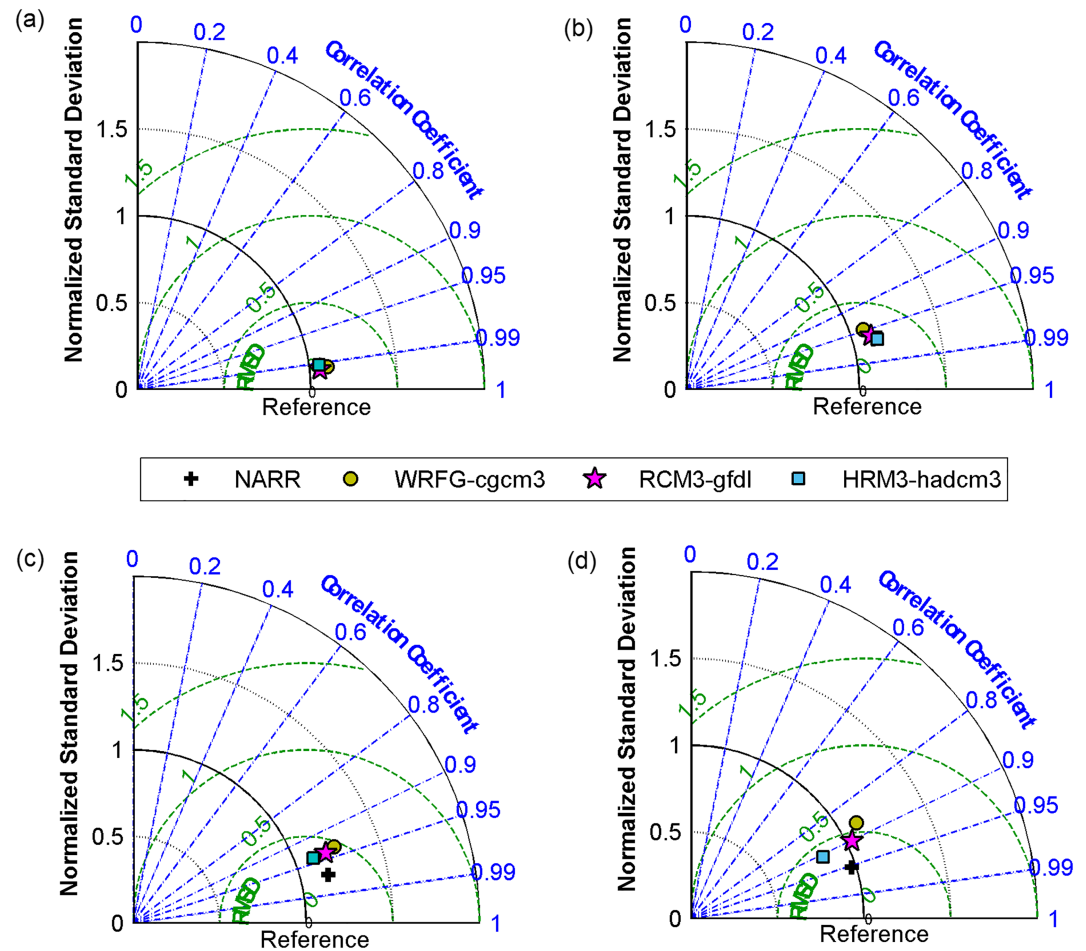


Figure 5. Taylor diagram for the time series for the bottom (a) and surface (b) O_2 concentration at CB4.3C ($38.56^\circ N$, $-76.43^\circ W$) and the hypoxic (c) and anoxic (d) volume. ROMS-RCA is forced by NARR and RCMs (WRFG_cgcm3, RCM3_gfdl, HRM3_hadcm3). Both the model fields and observation were interpolated to 1st and 15th of each calendar month.

straddles around 1, indicating that the model does a good job in reproducing the amplitude of variations in the observed time series. The model's performance is nearly as good as a hindcast simulation of 1989–1998 forced by the reanalysis product North American Regional Reanalysis and shows an improved skill when compared with previous modeling efforts (e.g., Irby et al., 2016).

By 2049–2058, O_2 declines nearly everywhere (Figures 4b, 4e, and 4h). The largest reduction appears in the subsurface water and in the lower bay. O_2 concentration shows a small reduction in the northern part of the hypoxic zone (between 38.6 and $39.1^\circ N$) in the model runs forced by WRFG_cgcm3 and RCM3_gfdl and even a slight increase in the model runs forced by HRM3_hadcm3. To better quantify the O_2 changes, we plotted the vertical profiles of O_2 concentration in the deep channel (>20 m; Figures 4c, 4f, and 4i). O_2 concentration shifts lower at all depths, with smaller decreases in the deep water.

Compared to the late 20th century, the hypoxic area in the mid-21st century expands seaward and upward (Figures 6a, 6d, and 6g). This leads to large increases in the hypoxic ($O_2 \leq 2 \text{ mg L}^{-1}$) and anoxic ($O_2 \leq 0.2 \text{ mg L}^{-1}$) volumes (Figures 6b, 6e, and 6h and Figures 6c, 6f, and 6i). These volumes were averaged over 1989–1998 and 2049–2058, respectively. For comparison, we also plotted the averaged observed hypoxic and anoxic volumes for 1989–1998. ROMS-RCA captured the observed seasonal variations of the hypoxic and anoxic volumes, although the model run forced by HRM3_hadcm3 underestimated the anoxic volume (Figure 6i). Despite intermodel differences, all the three model runs project substantial increases in the

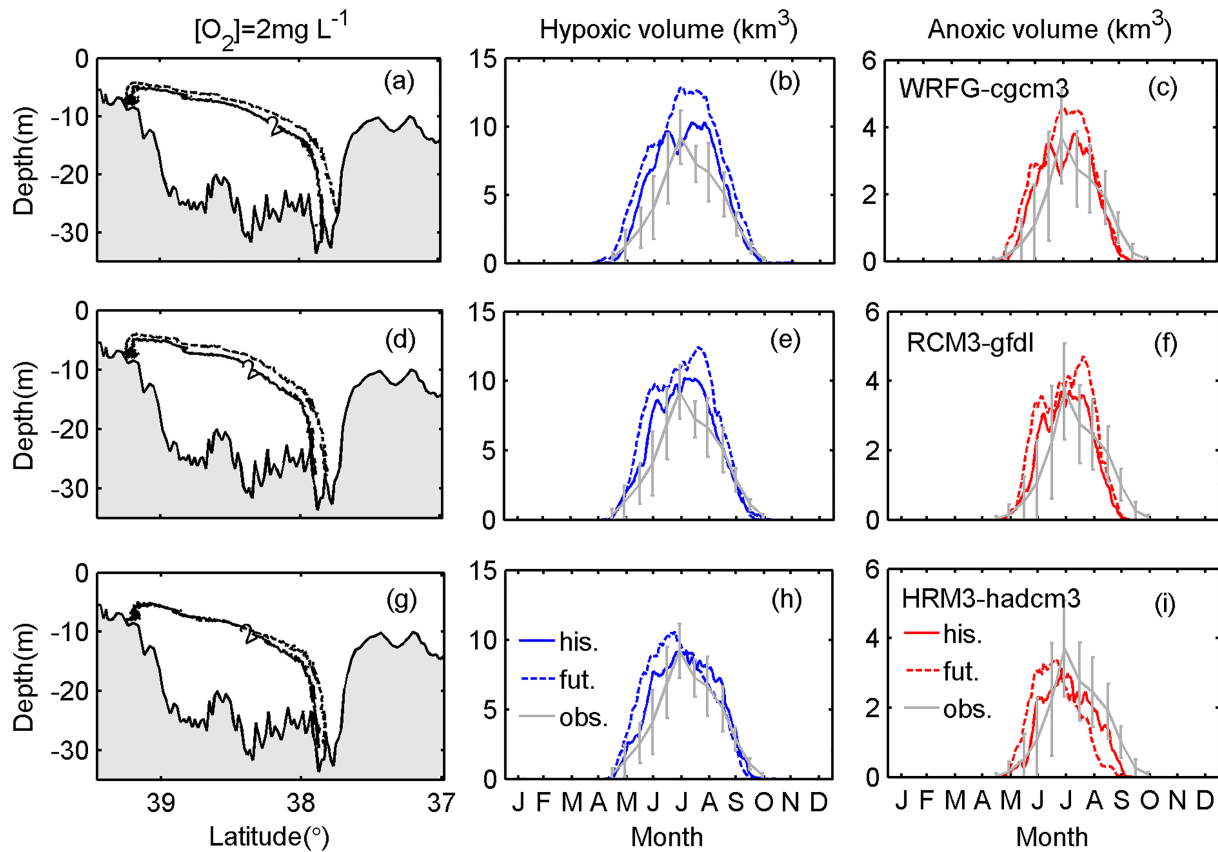


Figure 6. (a, d, g) Climatological mean position of the $O_2 = 2 \text{ mg L}^{-1}$ isoline in the along-channel section during the late 20th century (solid line) and mid-21st century (dashed line). Time series of the projected climatological mean hypoxic (second column) and anoxic (third column) volumes in Chesapeake Bay during the late 20th century (solid lines) and mid-21st century (dashed lines), projected by WRFG_cgcm3 (a–c), RCM3_gfdl (d–f), and HRM3_hadcm3 (g–i). The gray line indicates the mean and one standard deviation of the observed hypoxic and anoxic volumes during the late 20th century.

hypoxic and anoxic volumes in the future climate (Figure 6 and Table 3). WRFG_cgcm3 and RCM3_gfdl predict larger increases (20–30%), while HRM3_hadcm3 predicts smaller increases (~10%). The expansion of the hypoxic and anoxic volumes is significantly larger in early to midsummer (June–July) than in late summer (August and September). Another major change from the late 20th to the mid-21st century is the earlier initiation of hypoxia, from several days to nearly 2 weeks. RCM3_gfdl and HRM3_hadcm3 also project an earlier termination of hypoxia and a shorter hypoxia duration (Table 3).

3.2. Causes of Oxygen Decline

To determine the cause(s) for the O_2 decline, a diagnostic analysis was conducted of the O_2 budget in a fixed control volume V for the bottom water. V was selected to encompass all the waters below 10-m depth in the main stem of Chesapeake Bay, ranging between the Rappahannock River in the south and the Patapsco River in the north (Figure 1d). The O_2 budget over the control volume is derived from the full conservation equation given by

$$\frac{\partial O_2}{\partial t} = -u \frac{\partial O_2}{\partial x} - v \frac{\partial O_2}{\partial y} - w \frac{\partial O_2}{\partial z} + \frac{\partial}{\partial x} \left(K_H \frac{\partial O_2}{\partial x} \right) + \frac{\partial}{\partial y} \left(K_H \frac{\partial O_2}{\partial y} \right) + \frac{\partial}{\partial z} \left(K_V \frac{\partial O_2}{\partial z} \right) + WCR + SOD + F_{air-sea} + P_{phyto}, \quad (1)$$

where x , y , and z stand for the longitudinal (along-channel, namely, the major axis of the depth-averaged tidal flows), lateral (cross-channel), and vertical directions, respectively (see Xie et al., 2017 for a more detailed definition); u , v , and w represent the velocity components in these directions; K_H and K_V are the horizontal and vertical diffusivities, respectively; WCR is the water column O_2 uptake and includes algal

Table 3

Model Projections for the Seasonal Averaged Water Temperature, Winter-Spring Susquehanna River Flow (Averaged Over January–May), Relative Sea Level Rise (RSLR), Annual Cumulative and Averaged Summer (June–August) Hypoxic Volume (HV) and Anoxic Volume (AV), the Duration (Days), Initiation, and Termination Days of Hypoxia (Day of Year, Threshold is Set at 0.5 km³) in the Main Stem of Chesapeake Bay for the Late 20th and mid-21st Century

		WRFG_cgcm3			RCM3_gfdl			HRM3_hadcm3		
		Late 20th	Mid-21st	Change	Late 20th	Mid-21st	Change	Late 20th	Mid-21st	Change
Water temperature (°C)	Winter	6.3 (±0.7)	8.3 (±0.4)	2.0	6.1 (±0.7)	7.6 (±0.5)	1.5	6.1 (±0.8)	7.5 (±0.8)	1.4
	Spring	11.9 (±0.4)	13.6 (±0.7)	1.7	11.3 (±0.9)	12.2 (±0.7)	0.9	12.2 (±0.8)	12.9 (±1.0)	0.7
	Summer	24.8 (±0.3)	26.2 (±0.4)	1.4	24.1 (±0.5)	25.6 (±0.4)	1.5	25.1 (±0.6)	26.5 (±0.5)	1.4
	Fall	19.4 (±0.5)	21.2 (±0.6)	1.8	18.5 (±0.4)	20.1 (±0.5)	1.6	19.4 (±0.5)	21.1 (±0.4)	1.7
River flow (m ³ s ⁻¹)	Jan–May	1,794	2,045	251 (14%)	1,794	1,886	92 (5%)	1,794	2,237	443 (25%)
RSLR (m)		—	—	0.45	—	—	0.43	—	—	0.31
HV	Average (km ³)	8.5 (±1.3)	10.5 (±1.0)	2.0 (24%)	8.1 (±1.3)	10.0 (±1.4)	1.9 (23%)	7.6 (±1.3)	8.3 (±1.6)	0.7 (9%)
AV		2.7 (±0.8)	3.4 (±0.6)	0.6 (23%)	2.6 (±0.7)	3.4 (±0.8)	0.8 (29%)	2.1 (±0.7)	2.2 (±0.8)	0.4 (2%)
HV	Cumulative	943 (±161)	1,231 (±179)	288 (31%)	883 (±150)	1,092 (±196)	209 (24%)	857 (±123)	936 (±181)	79 (9%)
AV	(km ³ days)	273 (±76)	344 (±70)	71 (26%)	255 (±75)	330 (±87)	75 (29%)	209 (±59)	213 (±77)	4 (2%)
Onset	Day of year	132 (±9)	120 (±10)	−12	132 (±11)	131 (±10)	−1	129 (±5)	126 (±7)	−3
End		273 (±9)	274 (±11)	+1	271 (±9)	267 (±9)	−4	270 (±8)	265 (±10)	−5
Duration		141 (±11)	154 (±11)	+13	139 (±14)	136 (±13)	−3	141 (±8)	139 (±12)	−2

Note. The numbers in the parentheses indicate one standard deviation. The percentage numbers in the bracket are noted as relative change.

respiration, organic matter oxidation, nitrification, and oxidation of sulfide/methane; SOD is the sediment oxygen demand; $F_{air-sea}$ is O₂ flux across the air-sea interface; and P_{phyto} is O₂ produced by phytoplankton in the euphotic layer.

Integrating equation (1) over control volume V for the bottom water yields

$$\begin{aligned} \frac{\partial M_{O_2}}{\partial t} = & \underbrace{\iint_{A1} (-uO_2) dydz}_{F_{hadv}} + \underbrace{\iint_{A1} \left(K_H \frac{\partial O_2}{\partial x} \right) dydz}_{F_{hdiff}} + \iint (-vO_2) dx dz + \iint \left(K_H \frac{\partial O_2}{\partial y} \right) dx dz \\ & + \underbrace{\iint_{A2} (-wO_2) dx dy}_{F_{vadv}} + \underbrace{\iint_{A2} \left(K_V \frac{\partial O_2}{\partial z} \right) dx dy}_{F_{vdiff}} + \iiint_V (WCR) dx dy dz + \iint_{A3} (SOD) dx dy, \end{aligned} \quad (2)$$

where M_{O_2} is the total O₂ content (unit = kg) in V (Li et al., 2015). F_{hadv} and F_{hdiff} represent the horizontal advective and diffusive influxes of O₂ into the cross-channel section ($A1$) in the lower Bay. Since V intersects the bottom of the shallow upper Bay as well as the lateral boundary of the deep channel, the landward out-flux and lateral fluxes are zero there (third and fourth term in equation (2)). F_{vadv} and F_{vdiff} represent the vertical advective and diffusive fluxes across the upper boundary ($A2$) of V . WCR and SOD are integrated over V and the water-sediment interface ($A3$) separately. Since the euphotic layer depth in the estuary is typically shallower than the 10-m depth, O₂ production due to phytoplankton is very small in the bottom water and hence neglected in equation (2) (see also Li et al., 2015, 2016). As shown by Li et al. (2016), M_{O_2} in the control volume is highly negatively correlated with the hypoxic volume. Therefore, an analysis of the O₂ budget can tell us about the physical and biogeochemical processes driving the changes in the hypoxic and anoxic volumes.

Figure 7 shows the time series of monthly averaged F_{hadv} , F_{hdiff} , F_{vadv} , F_{vdiff} , WCR , and SOD for the two decades 1989–1998 and 2049–2058, obtained from the ROMS-RCA model run forced by WRFG_cgcm3. Over 1 year, three physical processes dominate the supply of O₂ to the bottom hypoxic water: The vertical diffusive F_{vdiff} and advective F_{vadv} fluxes supply O₂ to the bottom water while the horizontal advective flux F_{hadv} imports high-O₂ water in the lower Bay to the mid-Bay hypoxic region. Two biological terms WCR and SOD consume O₂, with WCR as the dominant consumption term. Between the late 20th and mid-21st century, F_{vdiff} , F_{vadv} , and WCR display the largest changes. During the summer, F_{vadv} decreases by 10%, and F_{vdiff} decreases by 18%, indicating that the vertical O₂ supply is reduced. F_{hadv} and F_{hdiff} have moderate

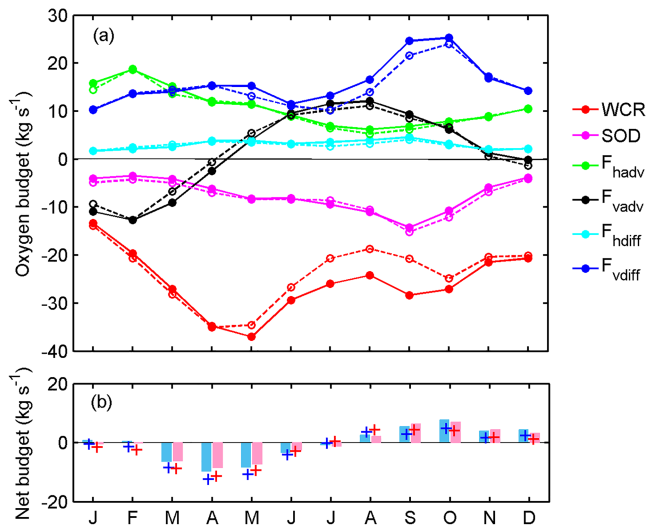


Figure 7. (a) Time series of the oxygen budget terms in the control volume during the late 20th century (solid lines with circles) and mid-21st century (dashed lines with circles), as projected by WRFG_cgcm3. (b) Time series of the sum of oxygen budget terms for the late 20th century (blue cross) and mid-21st century (red cross), compared with oxygen content change rate for the late 20th century (blue bar) and mid-21st century (red bar) in the control volume.

reductions. On the other hand, *WCR* is substantially smaller in the future climate while *SOD* shows a small reduction. Therefore, both the physical O_2 supply and biological consumption decrease with climate change. During the winter and early spring when biological production is weak, however, *WCR* and *SOD* show slight increases. The sum of the budget terms on the right-hand side of equation (2) for both simulation periods (1989–1998 and 2049–2058) is nearly the same as the rate of change in the O_2 content in the control volume, confirming that the numerical calculations of these budget terms are accurate.

The vertical advective and diffusive fluxes of O_2 are regulated by the strength of the vertical stratification (Li et al., 2015; Scully, 2010). With sea level rise and higher winter-spring river flow in the future climate (Figure 3 and Table 3), stratification in the estuary becomes stronger (Figure 8). The surface salinity increases by 0.5–1 psu, and the bottom salinity is 1–2 psu higher during summer (Figures 8a and 8b). In the along-channel section, saline bottom water penetrates further into the estuary while the brackish surface water spreads seaward in the lower bay (Figure 8d). The Brunt–Väisälä frequency (N^2) averaged over the estuary increases by $2.6 \times 10^{-4} s^{-2}$, with larger stratification increases on the shallow shoals than in the deep channel (Figures 8c and 9a). The stronger stratification suppresses turbulent mixing, resulting in weaker diffusive supply of O_2 to the bottom water in the future climate and the expansion of hypoxic region (Figure 9c).

It should be pointed out that the physical O_2 supply terms not only depend on the physical fields such as velocities and diffusivity but also depend on the O_2 concentration itself (see equation (2)). Part of the changes in F_{vdiff} and F_{vadv} could be related to the lower O_2 in the future climate. The reduction in the vertical diffusive flux F_{vdiff} is larger during summer (Figure 7) and is partly caused by the large O_2 decline in the surface layer and the associated weakening of the vertical O_2 gradient in the pycnocline (Figures 4b, 4e, and 4h). The horizontal advective flux F_{hadv} also decreases in the future climate. The estuarine circulation is moderately stronger in the future climate, in agreement with Hong and Shen (2012). However, the seaward expansion of

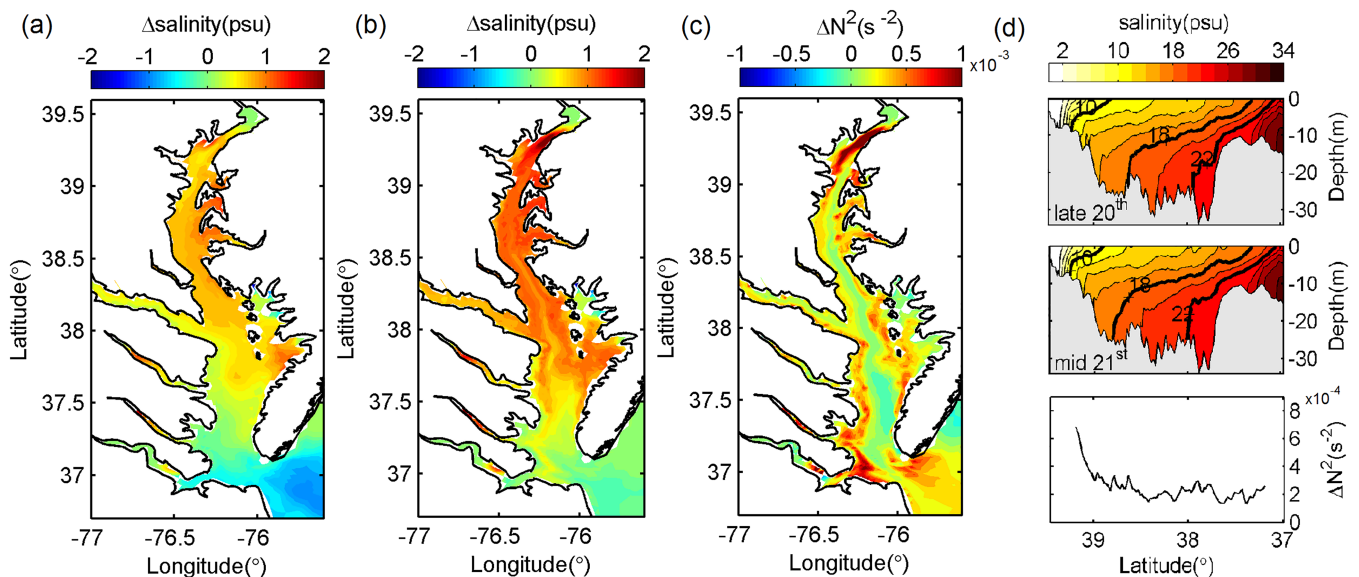


Figure 8. Changes in the summer averaged (a) surface salinity, (b) bottom salinity, and (c) vertically averaged buoyancy frequency N^2 between the late 20th century and mid-21st century, as projected in the model simulation forced by WRFG_cgcm3. (d) The summer-averaged along-channel salinity distribution in the late 20th century (upper panel) and mid-21st century (middle panel), and changes in the vertically averaged summer stratification N^2 (lower panel) between the two periods.

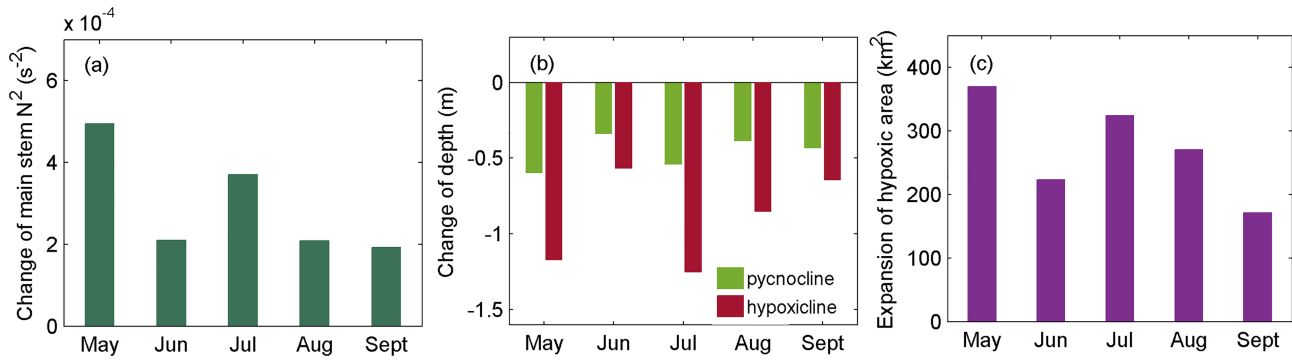


Figure 9. (a) Monthly averaged changes in buoyancy frequency N^2 over Chesapeake Bay from May to September. (b) Changes in the depth of pycnocline and hypoxic line (isoline of $O_2 = 2 \text{ mg L}^{-1}$) from May to September. (c) Increases in the hypoxic area from May to September, as projected in the model run forced by WRFG_cgcm3.

the hypoxic region and O_2 reduction in the lower Bay, as shown in Figures 4b, 4e, and 4h, lowers the O_2 concentration in the incoming water, such that F_{hadv} (a product of u and O_2) is reduced in the future climate.

Sea level rise may also contribute to worsening hypoxia in the future climate by increasing the volume of Chesapeake Bay and creating more space to develop hypoxia. To examine this, monthly averaged changes in the pycnocline depth and hypoxic-line depth (isoline of $O_2 = 2 \text{ mg L}^{-1}$) were calculated over the hypoxic region from May to September (Figure 9b). The pycnocline depth will be 0.3–0.6 m shallower, and hypoxic-line depth will be 1.25 m shallower, according to the model simulation forced by WRFG_cgcm3. Clearly, the hypoxic water is able to fill in the extra volume created by sea level rise. Furthermore, the greater shoaling of the hypoxic line relative to the pycnocline suggests that other processes such as *WCR* also contribute to the upward expansion of hypoxic water.

The water column respiration shows large decreases during the summer and small increases earlier in the year (Figure 7). *WCR* depends on the organic matter produced during the spring bloom. The winter-spring phytoplankton bloom terminates earlier (Figure 10a), and the total particulate organic carbon in the water column accumulates slightly faster during the spring (Figure 10b). Also, the temperature-dependent oxidation rate of organic matter in the water column and sediment is higher early in the year, resulting in an earlier onset of hypoxia. On the other hand, the summer phytoplankton biomass increases in early summer (May and June) but decreases in late summer and early fall (July to September; Figure 10a). With the projected warming from WRFG_cgcm3, the summer water temperature will reach $26.5 \text{ }^\circ\text{C}$, exceeding the

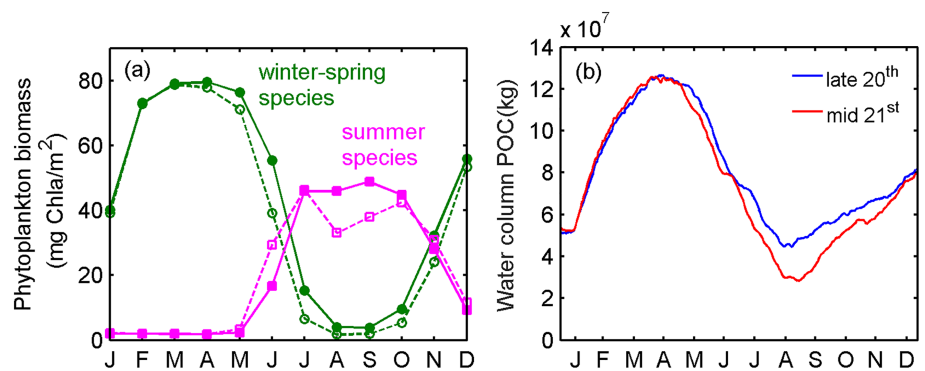


Figure 10. (a) Monthly averaged phytoplankton biomass in the euphotic layer during the late 20th century (solid lines) and mid-21st century (dashed lines) for the winter-spring species (green) and summer species (pink) as projected by WRFG_cgcm3. (b) Daily averaged total particulate organic carbon (POC) in the whole water column during the late 20th century (blue) and mid-21st century (red).

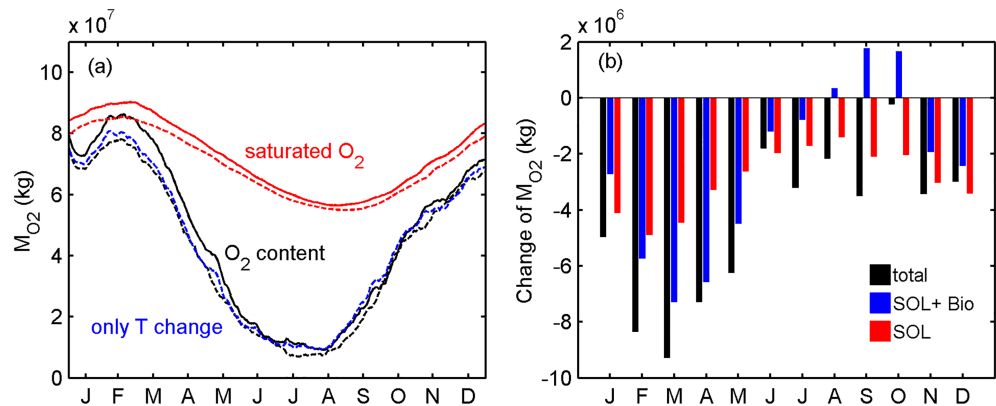


Figure 11. (a) The total oxygen content in the control volume (black) and hypothetical changes in the oxygen content due to solubility change (red) at the late 20th century (solid lines) and mid-21st century (dashed lines), as projected by WRFG_cgcm3. The blue line is the oxygen content calculated from a model run of the mid-21st century in which the full effects of temperature are simulated in RCA but the hydrodynamic field is kept the same as that in the historical simulation period. (b) Changes in the oxygen content of the control volume (black bar), changes due to solubility (red bar), and changes due to the combined effects of solubility and biological consumption (blue bar) between the late 20th century and mid-21st century.

optimal growth temperature (25 °C) for the summer phytoplankton species and suppressing their production. Less organic matter is produced for the export to deeper waters (Figure 10b), resulting in a large reduction in the summer *WCR* (Figure 7). These biogeochemical changes account for the earlier hypoxia onset and more rapid disintegration of hypoxia and anoxia seen in Figure 6.

In addition to the physical and biological factors discussed above, decreasing O₂ solubility could contribute to the expansion of hypoxia in the future climate. The solubility effect varies seasonally: larger O₂ reductions in winter and fall and smaller reductions in summer (Figure 11a). Over a year, the oxygen content change due to decreasing solubility accounts for about one half of the total reduction in the bottom-water oxygen content between late 20th century and mid-21st century (Figure 11b). Warming affects not only solubility but also biological consumption. We conducted an additional model run for the mid-21st century that simulates the full effects of temperature increase in the RCA biogeochemical model while keeping the same hydrodynamic field as that in the late 20th century. The O₂ difference between this hypothetical model run and the historical simulation thus represents the combined effects of solubility and biological consumption due to the temperature increase between late 20th century and mid-21st century (compare the blue and black dashed lines in Figure 11a). During the spring, O₂ loss due to higher biological consumption is comparable to that due to the reduced solubility. During the summer and early fall, however, the biological consumption decreases and offsets the O₂ loss due to solubility, resulting in a net O₂ gain (Figure 11b).

Given that both the physical supply and biological consumption decrease with climate change, why is the hypoxia more severe in the future climate? An examination of the overall balance among the various terms in the budget gives us some insights. Equation (2) was integrated over the entire year or over the summer (June–August) to produce the time-integrated budget terms (Figures 12a and 12c). All the physical supply terms decline in the future climate. The vertical diffusive flux experiences the largest reduction. Either the vertical advective flux or the horizontal advective flux has the second largest reduction, depending on whether the budget is integrated over the summer or the entire year. The two biological consumption terms also decrease in the future climate, with *WCR* being the bigger contributor. Despite the compensative changes in the physical supply and biological consumption, the O₂ content is lower in the mid-21st century than in the late 20th century (Figure 12b), consistent with the projected increases in the hypoxic and anoxic volumes (Figure 6). Next we compare the total change in the bottom-water O₂ content with that due to solubility change. The solubility-induced change is equivalent to 69% of the total content change during the summer but is larger when integrated over a year, presumably because of the large *WCR* reduction in late summer and fall. It should be pointed out that individual terms in the O₂ budget are ~1–2 orders larger than the net O₂ content change (term on the left hand of equation (2)) and the O₂ content loss due to solubility (cf.

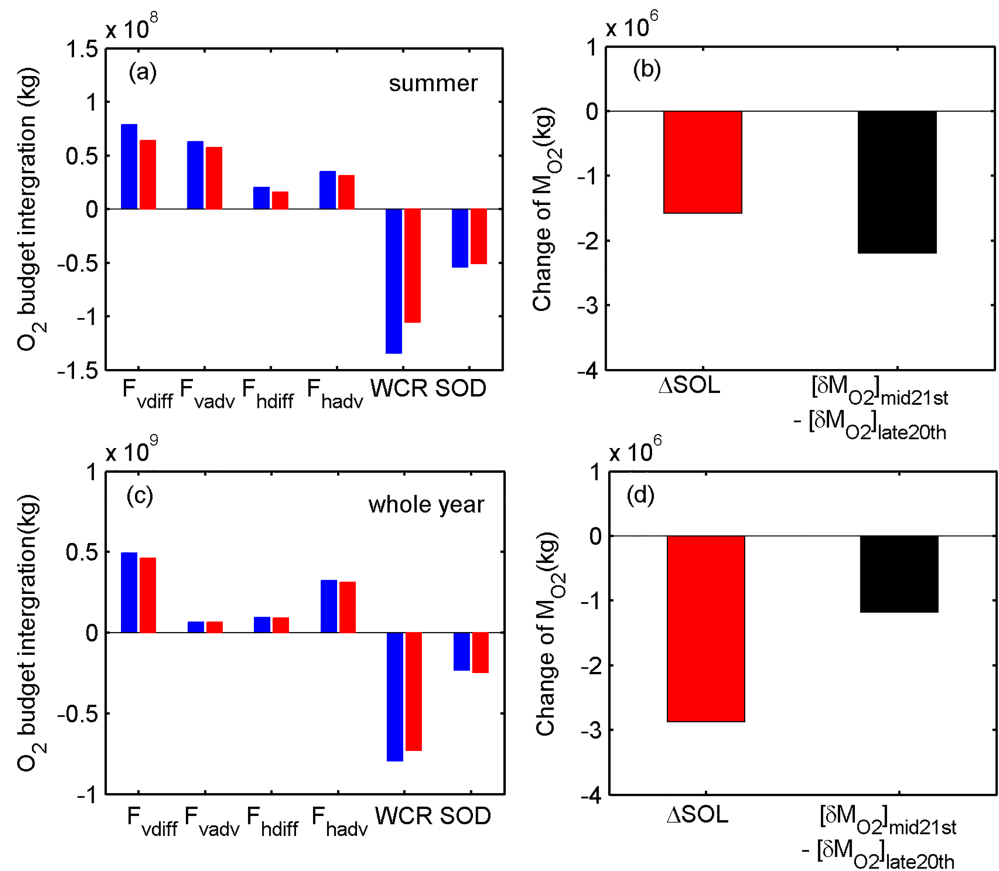


Figure 12. Integrated oxygen budget terms over the summer (a) and whole year (c) in the late 20th century (blue bars) and mid-21st century (red bars). The net change of oxygen content in the control volume (black bars) and the change of oxygen content due to solubility change (red bars) over summer (b) and whole year (d) between the late 20th century and mid-21st century.

Figures 12a and 12b). It also should be noted that the numerical evaluations of the O₂ budget terms contain a small (7%) error, but it is considerably smaller than the changes of the individual terms (see Figure 7b).

4. Discussion and Conclusion

In the open ocean, climate change brings about stronger upper-ocean stratification, reduced solubility, and increased microbial respiration, all pointing to increasing deoxygenation in the future climate. Moreover, decreasing solubility was found to be the dominant driver for the O₂ decline in the upper open ocean (Schmidtko et al., 2017). In contrast, our budget analysis of bottom-water O₂ in Chesapeake Bay reveals intriguingly different physical and biogeochemical responses to climate change in a eutrophic estuary. Using the downscaled climate projections and a coupled hydrodynamic-biogeochemical model, we projected that the hypoxic and anoxic volumes in Chesapeake Bay would increase by 10–30% between the late 20th and mid-21st century. Despite the differences among the three RCM projections, the projected increases in hypoxia in this eutrophic estuary are similar. This increase of 10–30% in the hypoxic and anoxic volumes is larger than the increases obtained from the model runs that considered simplified changes from climate model projections (Irby et al., 2018; Wang et al., 2017), suggesting possible nonlinear synergistic effects among different climate change factors.

The combined effects of sea level rise and larger winter-spring runoff lead to stronger stratification in the future climate, resulting in larger reductions in the vertical diffusive and advective O₂ fluxes to the bottom water. While turbulent mixing is known to be suppressed in stratified water, previous studies (Lerczak & Geyer, 2004; Scully, 2010; Li et al., 2015; Xie & Li, 2018) also showed that vertical advection due to lateral circulation decreases under stronger stratification. Therefore, one certain aspect about the impact of

climate change on estuarine hypoxia is the increasing stratification and decreasing vertical supply of O_2 to the bottom water. The import of high- O_2 coastal water by estuarine return flow is also a significant source of O_2 to the hypoxic region (Li et al., 2015, 2016). According to our analysis, F_{hadv} decreases in the future climate, primarily due to the seaward expansion of hypoxia and O_2 reduction in the lower Bay.

The simplified climate change numerical experiments by Wang et al. (2017) and Irby et al. (2018) showed that sea level rise amplifies the estuarine transport and leads to stronger import of higher- O_2 coastal water to the hypoxic region in the mid-Bay. The net effect of sea level rise on estuarine hypoxia ultimately depends on the competition between the stronger vertical stratification and stronger inflows and is the subject of an ongoing model intercomparison study. Also, these studies superimposed the projected sea level rise onto the sea level oscillations at the offshore boundary and did not consider the geomorphic change with sea level rise (e.g., inundation of low-lying land areas) and its effects on tidal dynamics and estuarine circulation.

Climate-induced shifts in phenology in marine ecosystems have been well documented (e.g., Edwards & Richardson, 2004; Kirby et al., 2007; Nixon et al., 2009). Our model shows the earlier shifts of both winter-spring and summer phytoplankton species (Figure 10), in concert with the earlier initiation of hypoxia in spring and more rapid disintegration of hypoxia in late summer and early fall. These results are consistent with a recent retrospective analysis of 30-year monitoring data in Chesapeake Bay by Testa et al. (2018) and Murphy et al. (2011). They observed an increase in winter phytoplankton biomass in landward regions, elevated early summer hypoxic volumes, and a decreasing trend of late summer hypoxia. Testa et al. (2018) found that warming led to elevated rates of organic matter degradation and “speeding-up” of the typical seasonal cycle. Similar climate warming effects were observed on terrestrial ecosystems and biogeochemistry over land (Elmore et al., 2016). In the ROMS-RCA model, the phytoplankton community is represented by two functional groups: winter-spring species and summer species. Warming leads to earlier bloom of the winter-spring species and smaller biomass of the summer species. Although the retrospective data analysis by Testa et al. (2018) is consistent with our model results, one cannot rule out the possibility that new plankton species able to tolerate higher temperature may migrate to Chesapeake Bay in the future climate (Barton et al., 2016). Should this happen, the water column respiration may increase during the summer season and drive more severe hypoxia.

While ocean warming and sea level rise were considered in this study, changes of nutrient concentration in the open ocean were not considered. Such nutrient changes were found to induce 20–30% reduction of biological production on the northwest European shelf as increased stratification in a warming climate reduced oceanic nutrient supply (Gröger et al., 2013; Holt et al., 2012). However, in a eutrophic estuary like Chesapeake Bay, the nutrient loading from the rivers is 1–2 orders of magnitude larger than the nutrient input from the adjacent ocean (Nixon, 1987; Kemp et al., 2005). Nutrient concentration changes in the open ocean are expected to have a minor effect on hypoxia in this estuary. Nevertheless, the northward shift of Gulf Stream, which is not fully resolved in the oceanic GCMs, may cause a greater reduction in oxygen solubility in the northwest Atlantic shelf (Claret et al., 2018). This may decrease O_2 concentration in the incoming bottom water from the shelf and exacerbate the hypoxic condition in Chesapeake Bay.

This study did not consider the effects of nutrient reductions that might be implemented to meet water quality standards. When the mandated nutrient reductions for Chesapeake Bay were considered, Irby et al. (2018) found that the negative impacts of climate change in 2050 were significantly smaller than improvements in O_2 due to the nutrient reduction. Saraiva et al. (2019a) reached a similar conclusion when studying the combined effects of changing nutrient loads from land and changing climate on the Baltic Sea during the 21st century. It would be interesting to extend our study to include the effects of different nutrient-reduction scenarios in the future.

Our goal here is not only to make climate downscaling projections on Chesapeake Bay hypoxia but also to gain better understanding of physical and biogeochemical controls of hypoxia under climate change. To make robust future projections, particularly for the late 21st century when the range of climate change scenarios is much wider, one would need to expand the uncertainty analysis by including more greenhouse gas concentration scenarios and nutrient loading scenarios, as done recently for the Baltic Sea by Saraiva et al. (2019b).

Acknowledgments

We thank two anonymous reviewers for their helpful comments. We are grateful to NSF (CBET-1360285), NOAA-OAP (NA15NOS4780184) and Pennsylvania Sea Grant (NA10OAR4170063) for the financial support. Data can be downloaded online (<https://doi.org/10.5281/zenodo.3352248>). This is UMCES contribution number 5720.

References

- Altieri, A., & Gedan, K. B. (2015). Climate change and dead zones. *Global Change Biology*, *21*(4), 1395–1406. <https://doi.org/10.1111/gcb.12754>
- Barton, A. D., Irwin, A. J., Finkel, Z. V., & Stock, C. A. (2016). Anthropogenic climate change drives shift and shuffle in North Atlantic phytoplankton communities. *Proceedings of the National Academy of Sciences*, *113*(11), 2964–2969. <https://doi.org/10.1073/pnas.1519080113>
- Bendtsen, J., & Hansen, J. L. S. (2013). Effects of global warming on hypoxia in the Baltic Sea–North Sea transition zone. *Ecological Modelling*, *264*, 17–26. <https://doi.org/10.1016/j.ecolmodel.2012.06.018>
- Boesch, D. F., Atkinson, L. P., Boicourt, W. C., Boon, J. D., Cahoon, D. R., Dalrymple, R. A., et al. (2013). *Updating Maryland's sea-level rise projections: Special report of the Scientific and Technical Working Group to the Maryland Climate Change Commission* (p. 22). Cambridge, MD: University of Maryland Center for Environmental Science.
- Boon, J. D., & Mitchell, M. (2015). Nonlinear change in sea level observed at North American tide stations. *Journal of Coastal Research*, *31*(6), 1295–1305.
- Brady, D. C., Testa, J. M., Di Toro, D. M., Boynton, W. R., & Kemp, W. M. (2013). Sediment flux modeling: Calibration and application for coastal systems. *Estuarine, Coastal and Shelf Science*, *117*, 107–124. <https://doi.org/10.1016/j.ecss.2012.11.003>
- Breitburg, D., Levin, L. A., Oschlies, A., Grégoire, M., Chavez, F. P., Conley, D. J., et al. (2018). Declining oxygen in the global ocean and coastal waters. *Science*, *359*(6371), eaam7240. <https://doi.org/10.1126/science.aam7240>
- Caya, D., & Laprise, R. (1999). A semi-Lagrangian semi-implicit regional climate model: The Canadian RCM. *Monthly Weather Review*, *127*(3), 341–362. [https://doi.org/10.1175/1520-0493\(1999\)127<0341:ASISLR>2.0.CO;2](https://doi.org/10.1175/1520-0493(1999)127<0341:ASISLR>2.0.CO;2)
- Chapman, D. C., & Beardsley, R. C. (1989). On the origin of shelf water in the middle Atlantic Bight. *Journal of Physical Oceanography*, *19*(3), 384–391. [https://doi.org/10.1175/1520-0485\(1989\)019<0384:OTOOSW>2.0.CO;2](https://doi.org/10.1175/1520-0485(1989)019<0384:OTOOSW>2.0.CO;2)
- Claret, M., Galbraith, E. D., Palter, J. B., Bianchi, D., Fennel, K., Gilbert, D., & Dunne, J. P. (2018). Rapid coastal deoxygenation due to ocean circulation shift in the northwest Atlantic. *Nature Climate Change*, *8*(10), 868–872. <https://doi.org/10.1038/s41558-018-0263-1>
- Collins, W. D., Bitz, C. M., Blackmon, M. L., Bonan, G. B., Bretherton, C. S., Carton, J. A., et al. (2006). The community climate system model version 3 (CCSM3). *Journal of Climate*, *19*(11), 2122–2143. <https://doi.org/10.1175/JCLI3761.1>
- Delworth, T. L., Broccoli, A. J., Rosati, A., Stouffer, R. J., Balaji, V., Beesley, J. A., et al. (2006). GFDL's CM2 global coupled climate models. Part I: Formulation and simulation characteristics. *Journal of Climate*, *19*, 643–674. <https://doi.org/10.1175/JCLI3629.1>
- Deutsch, C., Brix, H., Ito, T., Frenzel, H., & Thompson, L. (2011). Climate-forced variability of ocean hypoxia. *Science*, *333*(6040), 336–339. <https://doi.org/10.1126/science.1202422>
- Di Toro, D. M. (2001). *Sediment flux modeling* (p. 624). New York: Wiley-Interscience.
- Diaz, R. J., & Rosenberg, R. (2008). Spreading dead zones and consequences for marine ecosystems. *Science*, *321*(5891), 926–929. <https://doi.org/10.1126/science.1156401>
- Ding, H., & Elmore, A. J. (2015). Spatio-temporal patterns in water surface temperature from Landsat time series data in the Chesapeake Bay, USA. *Remote Sensing of Environment*, *168*, 335–348. <https://doi.org/10.1016/j.rse.2015.07.009>
- Du, J., Shen, J., Park, K., Wang, Y. P., & Yu, X. (2018). Science of the Total Environment Worsened physical condition due to climate change contributes to the increasing hypoxia in Chesapeake Bay. *Science of Total Environment*, *630*, 707–717. <https://doi.org/10.1016/j.scitotenv.2018.02.265>
- Edwards, M., & Richardson, A. J. (2004). Impact of climate change on marine pelagic phenology and trophic mismatch. *Nature*, *430*(7002), 881–884. <https://doi.org/10.1038/nature02808>
- Egbert, G. D., & Erofeeva, S. Y. (2002). Efficient inverse modeling of barotropic ocean tides. *Journal of Atmospheric and Oceanic Technology*, *19*(2), 183–204. [https://doi.org/10.1175/1520-0426\(2002\)019<0183:EIMOBO>2.0.CO;2](https://doi.org/10.1175/1520-0426(2002)019<0183:EIMOBO>2.0.CO;2)
- Elmore, A. J., Nelson, D. M., & Craine, J. M. (2016). Earlier springs are causing reduced nitrogen availability in North American eastern deciduous forests. *Nature Plants*, *2*(10), 1–5. <https://doi.org/10.1038/nplants.2016.133>
- Fairall, C. W., Bradley, E. F., Hare, J. E., Grachev, A. A., & Edson, J. B. (2003). Bulk parameterization of air–sea fluxes: Updates and verification for the COARE algorithm. *Journal of Climate*, *16*(4), 571–591. [https://doi.org/10.1175/1520-0442\(2003\)016<0571:BPOASF>2.0.CO;2](https://doi.org/10.1175/1520-0442(2003)016<0571:BPOASF>2.0.CO;2)
- Feng, Y., DiMarco, S. F., & Jackson, G. A. (2012). Relative role of wind forcing and riverine nutrient input on the extent of hypoxia in the northern Gulf of Mexico. *Geophysical Research Letters*, *39*, L09601. <https://doi.org/10.1029/2012GL051192>
- Fennel, K., & Testa, J. M. (2019). Biogeochemical controls on coastal hypoxia. *Annual Review of Marine Science*, *11*(4), 1–26. <https://doi.org/10.1146/annurev-marine-010318-095138-095138>
- Fennel, K., Wilkin, J., Levin, J., Moisan, J., O'Reilly, J., & Haidvogel, D. (2006). Nitrogen cycling in the Middle Atlantic Bight: Results from a three-dimensional model and implications for the North Atlantic nitrogen budget. *Global Biogeochemical Cycles*, *20*, GB3007. <https://doi.org/10.1029/2005GB002456>
- Filippino, K. C., Mulholland, M. R., & Bernhardt, P. W. (2011). Nitrogen uptake and primary productivity rates in the Mid-Atlantic Bight (MAB). *Estuarine, Coastal and Shelf Science*, *91*(1), 13–23. <https://doi.org/10.1016/j.ecss.2010.10.001>
- Flato, G. M. (2005). The third generation Coupled Global Climate Model (CGCM3). Environment Canada Canadian Centre for Climate Modelling and Analysis note. Retrieved from <http://www.ec.gc.ca/ccmac-cccma/default.asp?n=1299529F-1>
- GFDL Global Atmospheric Model Development Team (2004). The new GFDL global atmospheric and land model AM2-LM2: Evaluation with prescribed SST simulations. *Journal of Climate*, *17*(24), 4641–4673. <https://doi.org/10.1175/JCLI-3223.1>
- Gilbert, D., Rabalais, N. N., Diaz, R. J., & Zhang, J. (2010). Evidence for greater oxygen decline rates in the coastal ocean than in the open ocean. *Biogeosciences*, *7*(7), 2283–2296. <https://doi.org/10.5194/bg-7-2283-2010>
- Giorgi, F., & Gutowski, W. J. Jr. (2015). Regional dynamical downscaling and the CORDEX initiative. *Annual Review of Environment and Resources*, *40*(1), 467–490. <https://doi.org/10.1146/annurev-environ-102014-021217>
- Giorgi, F., Marinucci, M. R., & Bates, G. T. (1993). Development of a second-generation regional climate model (RegCM2). Part I: Boundary-layer and radiative transfer processes. *Monthly Weather Review*, *121*(10), 2794–2813. [https://doi.org/10.1175/1520-0493\(1993\)121<2794:DOASGR>2.0.CO;2](https://doi.org/10.1175/1520-0493(1993)121<2794:DOASGR>2.0.CO;2)
- Giorgi, F., Marinucci, M. R., Bates, G. T., & De Canio, G. (1993). Development of a second-generation regional climate model (RegCM2). Part II: Convective processes and assimilation of lateral boundary conditions. *Monthly Weather Review*, *121*(10), 2814–2832. [https://doi.org/10.1175/1520-0493\(1993\)121<2814:DOASGR>2.0.CO;2](https://doi.org/10.1175/1520-0493(1993)121<2814:DOASGR>2.0.CO;2)
- Gordon, C., Cooper, C., Senior, C. A., Banks, H., Gregory, J. M., Johns, T. C., et al. (2000). The simulation of SST, sea ice extents and ocean heat transports in a version of the Hadley Centre coupled model without flux adjustments. *Climate Dynamics*, *16*(2–3), 147–168. <https://doi.org/10.1007/s003820050010>

- Grell, G. A., Dudhia, J., & Stauffer, D. R. (1993). A description of the fifth-generation Penn State/NCAR mesoscale model (MM5). NCAR Tech. Note NCAR/TN-398, 107 pp.
- Gröger, M., Maier-Reimer, E., Mikolajewicz, U., Moll, A., & Sein, D. (2013). NW European shelf under climate warming: Implications for open ocean–shelf exchange, primary production, and carbon absorption. *Biogeosciences*, *10*(6), 3767–3792. <https://doi.org/10.5194/bg-10-3767-2013>
- Große, F., Greenwood, N., Kreus, M., Lenhart, H.-J., Machoczek, D., Pätsch, J., et al. (2016). Looking beyond stratification: A model-based analysis of the biological drivers of oxygen deficiency in the North Sea. *Biogeosciences*, *13*(8), 2511–2535. <http://doi.org/10.5194/bg-13-2511-2016>
- Gudmundsson, L., Bremnes, J. B., & Haugen, J. E. (2012). Technical Note: Downscaling RCM precipitation to the station scale using statistical transformations—A comparison of methods. *Hydrology and Earth System Sciences*, *16*(9), 3383–3390. <https://doi.org/10.5194/hess-16-3383-2012>
- Hagy, J. D., Boynton, W. R., Keefe, C. W., & Wood, K. V. (2004). Hypoxia in Chesapeake Bay, 1950–2001: Long-term change in relation to nutrient loading and river flow. *Estuaries*, *27*(4), 634–658. <https://doi.org/10.1007/BF02907650>
- Haidvogel, D. B., Arango, H., Budgell, W. P., Cornuelle, B. D., Curchitser, E., Di Lorenzo, E., et al. (2008). Ocean forecasting in terrain-following coordinates: Formulation and skill assessment of the regional ocean modeling system. *Journal of Computational Physics*, *227*(7), 3595–3624. <https://doi.org/10.1016/j.jcp.2007.06.016>
- Holt, J. T., Butenschon, M., Wakelin, S. L., Artioli, Y., & Allen, J. I. (2012). Oceanic controls on the primary production of the northwest European continental shelf: Model experiments under recent past conditions and a potential future scenario. *Biogeosciences*, *9*(1), 97–117. <https://doi.org/10.5194/bg-9-97-2012>
- Hong, B., & Shen, J. (2012). Responses of estuarine salinity and transport processes to potential future sea-level rise in the Chesapeake Bay. *Estuarine, Coastal and Shelf Science*, *104*, 33–45.
- Howarth, R. W., Swaney, D. P., Boyer, E. W., Marino, R., Jaworski, N., & Goodale, C. (2006). The influence of climate on average nitrogen export from large watersheds in the Northeastern United States. *Biogeochemistry*, *79*(1–2), 163–186. <https://doi.org/10.1007/s10533-006-9010-1>
- Irby, I. D., Friedrichs, M. A., Friedrichs, C. T., Bever, A., Hood, R. R., Lanerolle, L. W., et al. (2016). Challenges associated with modeling low-oxygen waters in Chesapeake Bay: A multiple model comparison. *Biogeosciences*, *13*(7), 2011–2028. <https://doi.org/10.5194/bg-13-2011-2016>
- Irby, I. D., Friedrichs, M. A. M., Da, F., & Hinson, K. E. (2018). The competing impacts of climate change and nutrient reductions on dissolved oxygen in Chesapeake Bay. *Biogeosciences*, *15*(9), 2649–2668. <https://doi.org/10.5194/bg-15-2649-2018>
- Isleib, R. P. E., Fitzpatrick, J. J., & Mueller, J. (2007). The development of a nitrogen control plan for a highly urbanized tidal embayment. *Proceedings of the Water Environment Federation*, *5*, 296–320.
- Jones, R., Hassell, D., Hudson, D., Wilson, S., Jenkins, G., & Mitchell, J. (2003). *Generating high resolution climate change scenarios using PRECIS* (p. 34). Bracknell, UK: UNDP National Communications Unit Workbook.
- Juang, H. M. H., Hong, S. Y., & Kanamitsu, M. (1997). The NCEP regional spectral model: An update. *Bulletin of the American Meteorological Society*, *78*(10), 2125–2143. [https://doi.org/10.1175/1520-0477\(1997\)078<2125:TNRMSA>2.0.CO;2](https://doi.org/10.1175/1520-0477(1997)078<2125:TNRMSA>2.0.CO;2)
- Justic, D., Rabalais, N. N., & Turner, R. E. (2002). Modeling the impacts of decadal changes in riverine nutrient fluxes on coastal eutrophication near the Mississippi River Delta. *Ecological Modelling*, *152*(1), 33–46. [https://doi.org/10.1016/S0304-3800\(01\)00472-0](https://doi.org/10.1016/S0304-3800(01)00472-0)
- Justic, D., Rabalais, N. N., & Turner, R. E. (2003). Simulated responses of the Gulf of Mexico hypoxia to variations in climate and anthropogenic nutrient loading. *Journal of Marine Systems*, *42*(3–4), 115–126. [https://doi.org/10.1016/S0924-7963\(03\)00070-8](https://doi.org/10.1016/S0924-7963(03)00070-8)
- Keeling, R. F., Arne, K., & Gruber, N. (2010). Ocean deoxygenation in a warming world. *Annual Review of Marine Science*, *2*, 199–229. <https://doi.org/10.1146/annurev.marine.010908.163855>
- Kemp, W. M., Boynton, W. R., Adolf, J. E., Boesch, D. F., Boicourt, W. C., Brush, G., et al. (2005). Eutrophication of Chesapeake Bay: Historical trends and ecological interactions. *Marine Ecology Progress Series*, *303*, 1–29. <https://doi.org/10.3354/meps303001>
- Kemp, W. M., Smith, E. M., Marvin-DiPasquale, M., & Boynton, W. R. (1997). Organic carbon balance and net ecosystem metabolism in Chesapeake Bay. *Marine Ecology Progress Series*, *150*, 229–248. <https://doi.org/10.3354/meps150229>
- Kemp, W. M., Testa, J. M., Conley, D. J., Gilbert, D., & Hagy, J. D. (2009). Temporal responses of coastal hypoxia to nutrient loading and physical controls. *Biogeochemistry*, *6*, 2985–3008.
- Kirby, R. R., Beaugrand, G., & Lindley, J. a, Richardson, A. J., Edwards, M., & Reid, P. C. (2007). Climate effects and benthic–pelagic coupling in the North Sea Climate effects and benthic–pelagic coupling in the North Sea. *Marine Ecology Progress Series*, *330*, 31–38. <https://doi.org/10.3354/meps330031>
- Laurent, A., Fennel, K., Ko, D. S., & Lehrter, J. (2018). Climate change projected to exacerbate impacts of coastal eutrophication in the northern Gulf of Mexico. *Journal of Geophysical Research: Oceans*, *123*, 1–19. <https://doi.org/10.1002/2017JC013583>
- Lee, S. B., Li, M., & Zhang, F. (2017). Impact of sea level rise on tidal range in Chesapeake and Delaware Bays. *Journal of Geophysical Research: Oceans*, *122*, 3917–3938. <https://doi.org/10.1002/2016JC012597>
- Lerczak, J. A., & Geyer, W. R. (2004). Modeling the lateral circulation in straight, stratified estuaries. *Journal of Physical Oceanography*, *34*(6), 1410–1428. [https://doi.org/10.1175/1520-0485\(2004\)034<1410:MTLCIS>2.0.CO;2](https://doi.org/10.1175/1520-0485(2004)034<1410:MTLCIS>2.0.CO;2)
- Levin, L. A. (2018). Manifestation, drivers, and emergence of open ocean deoxygenation. *Annual Review of Marine Science*, *10*, 229–260. <https://doi.org/10.1146/annurev-marine-121916-063359>
- Li, M., Lee, Y. J., Testa, J. M., Li, Y., Ni, W., Kemp, W. M., & Di Toro, D. M. (2016). What drives interannual variability of hypoxia in Chesapeake Bay: Climate forcing versus nutrient loading? *Geophysical Research Letters*, *43*, 2127–2134. <https://doi.org/10.1002/2015GL067334>
- Li, M., Zhong, L., & Boicourt, W. C. (2005). Simulations of Chesapeake Bay estuary: Sensitivity to turbulence mixing parameterizations and comparison with observations. *Journal of Geophysical Research*, *110*, C12004. <https://doi.org/10.1029/2004JC002585>
- Li, Y., Li, M., & Kemp, W. M. (2015). A budget analysis of bottom-water dissolved oxygen in Chesapeake Bay. *Estuaries and Coasts*, *38*(6), 2132–2148. <https://doi.org/10.1007/s12237-014-9928-9>
- Linker, L. C., Batiuk, R. A., Shenk, G. W., & Cerco, C. F. (2013). Development of the Chesapeake Bay watershed total maximum daily load allocation. *Journal of the American Water Resources Association*, *49*(5), 986–1006. <https://doi.org/10.1111/jawr.12105>
- Mearns, L. O., Arritt, R., Biner, S., Bukovsky, M. S., McGinnis, S., Sain, S., et al. (2012). The North American Regional Climate Change Assessment Program: Overview of phase I results. *Bulletin of the American Meteorological Society*, *93*(9), 1337–1362. <https://doi.org/10.1175/BAMS-D-11-00223.1>
- Mearns, L. O., Gutowski, W. J., Jones, R., Leung, L.-Y., McGinnis, S., Nunes, A. M. B., & Qian, Y. (2007, updated 2014). *The North American Regional Climate Change Assessment Program dataset*. Boulder, CO: National Center for Atmospheric Research Earth System Grid data portal. <https://doi.org/10.5065/D6RN35ST>

- Mearns, L. O., Sain, S., Leung, L. R., Bukovsky, M. S., McGinnis, S., Biner, S., et al. (2013). Climate change projections of the North American Regional Climate Change Assessment Program (NARCCAP). *Climatic Change*, *120*(4), 965–975. <https://doi.org/10.1007/s10584-013-0831-3>
- Meier, H. E. M., Andersson, H. C., Eilola, K., Gustafsson, B. G., Kuznetsov, I., Müller-Karulis, B., et al. (2011). Hypoxia in future climates: A model ensemble study for the Baltic Sea. *Geophysical Research Letters*, *38*, L24608. <https://doi.org/10.1029/2011GL049929>
- Meire, L., Soetaert, K. E. R., & Meysman, F. J. R. (2013). Impact of global change on coastal oxygen dynamics and risk of hypoxia. *Biogeosciences*, *10*(4), 2633–2653. <https://doi.org/10.5194/bg-10-2633-2013>
- Mesinger, F., DiMego, G., Kalnay, E., Mitchell, K., Shafran, P. C., Ebisuzaki, W., et al. (2006). North American Regional Reanalysis. *Bulletin of the American Meteorological Society*, *87*(3), 343–360. <https://doi.org/10.1175/BAMS-87-3-343>
- Miller, K. G., Kopp, R. E., Horton, B. P., Browning, J. V., & Kemp, A. C. (2013). A geological perspective on sea-level rise and its impacts along the U.S. mid-Atlantic coast. *Earth's Future*, *1*(1), 3–18. <https://doi.org/10.1002/2013EF000135>
- Milly, P. C. D., & Dunne, K. A. (2011). On the hydrologic adjustment of climate-model projections: The potential pitfall of potential evapotranspiration. *Earth Interactions*, *15*, 1–14. <http://doi.org/10.1175/2010EI363.1>
- Mitrovica, J. X., Gomez, N., & Clark, P. U. (2009). The sea-level fingerprint of west Antarctic collapse. *Science*, *323*(5915), 753. <https://doi.org/10.1126/science.1166510>
- Mitrovica, J. X., Gomez, N., Morrow, E., Hay, C., Latychev, K., & Tamisiea, M. E. (2011). On the robustness of predictions of sea level fingerprints. *Geophysical Journal International*, *187*(2), 729–742. <https://doi.org/10.1111/j.1365-246X.2011.05090.x>
- Morrison, J., Callendar, W., Foreman, M. G. G., Masson, D., & Fine, I. (2014). A model simulation of future oceanic conditions along the British Columbia continental shelf. Part I: Forcing fields and initial conditions. *Atmosphere-Ocean*, *52*(1), 1–19. <https://doi.org/10.1080/07055900.2013.868340>
- Murphy, R. R., Kemp, W. M., & Ball, W. P. (2011). Long-term trends in Chesapeake Bay seasonal hypoxia, stratification, and nutrient loading. *Estuaries and Coasts*, *34*(6), 1293–1309. <https://doi.org/10.1007/s12237-011-9413-7>
- Najjar, R. G., Pyke, C. R., Adams, M. B., Breitburg, D., Hershner, C., Kemp, M., et al. (2010). Potential climate-change impacts on the Chesapeake Bay. *Estuarine, Coastal and Shelf Science*, *86*(1), 1–20. <https://doi.org/10.1016/j.ecss.2009.09.026>
- Nakićenović, N., Alcamo, J., Davis, G., de Vries, B., Fenhann, J., Gaffin, S., et al. (2000). *Emission scenarios. A Special Report of Working Group III of the Intergovernmental Panel on Climate Change* (p. 599). Cambridge, UK: Cambridge University Press.
- Nixon, S. W. (1987). Chesapeake Bay nutrient budgets—A reassessment. *Biogeochemistry*, *4*(1), 77–90. <https://doi.org/10.1007/BF02187363>
- Nixon, S. W., Fulweiler, R. W., Buckley, B. A., Granger, S. L., Nowicki, B. L., & Henry, K. M. (2009). The impact of changing climate on phenology, productivity, and benthic-pelagic coupling in Narragansett Bay. *Estuarine, Coastal and Shelf Science*, *82*(1), 1–18. <https://doi.org/10.1016/j.ecss.2008.12.016>
- Pal, J. S., Giorgi, F., Bi, X., Elguindi, N., Solmon, F., Gao, X., et al. (2007). Regional climate modeling for the developing world: The ICTP RegCM3 and RegCM3. *Bulletin of American Meteorological Society*, *88*(9), 1395–1410. <https://doi.org/10.1175/BAMS-88-9-1395>
- Pal, J. S., Small, E. E., & Eltahir, E. A. (2000). Simulation of regional-scale water and energy budgets: Representation of subgrid cloud and precipitation processes within RegCM. *Journal of Geophysical Research*, *105*(D24), 29,579–29,594. <https://doi.org/10.1029/2000JD900415>
- Pope, V. D., Gallani, M. L., Rowntree, P. R., & Stratton, R. A. (2000). The impact of new physical parametrizations in the Hadley Centre climate model: HadAM3. *Climate Dynamics*, *16*(2-3), 123–146. <https://doi.org/10.1007/s003820050009>
- Rabalais, N., Conley, J., Slomp, P., & Turner, E. (2014). Eutrophication-driven deoxygenation in the coastal ocean. *Oceanography*, *27*(1), 172–183. <https://doi.org/10.5670/oceanog.2014.21>
- Rice, K. C., & Jastram, J. D. (2015). Rising air and stream-water temperatures in Chesapeake Bay region, USA. *Climatic Change*, *128*(1-2), 127–138. <https://doi.org/10.1007/s10584-014-1295-9>
- Saba, V. S., Griffies, S. M., Anderson, W. G., Winton, M., Alexander, M. A., Delworth, T. L., et al. (2016). Enhanced warming of the Northwest Atlantic Ocean under climate change. *Journal of Geophysical Research: Oceans*, *121*, 118–132. <https://doi.org/10.1002/2015JC011346>
- Saraiva, S., Meier, H. E. M., Andersson, H., Höglund, A., Dieterich, C., Groger, M., et al. (2019a). Baltic Sea ecosystem response to various nutrient load scenarios in present and future climates. *Climate Dynamics*, *52*, 3369–3387. <https://doi.org/10.1007/s00382-01804330-0>
- Saraiva, S., Meier, H. E. M., Andersson, H., Höglund, A., Dieterich, C., Hordoir, R., & Eilola, K. (2019b). Uncertainties in projections of the baltic sea ecosystem driven by an ensemble of global climate models. *Frontiers in Earth Science*, *6*, 244. <https://doi.org/10.3389/feart.2018.00244>
- Schaefer, S., & Alber, M. (2007). Temperature controls a latitudinal gradient in the proportion of watershed nitrogen exported to coastal ecosystems. *Biogeochemistry*, *85*, 333–346. <https://doi.org/10.1007/s10533-007-9144-9>
- Schmidtko, S., Stramma, L., & Visbeck, M. (2017). Decline in global oceanic oxygen content during the past five decades. *Nature*, *542*(7641), 335–339. <https://doi.org/10.1038/nature21399>
- Scinocca, J. F., & McFarlane, N. A. (2004). The variability of modeled tropical precipitation. *Journal of the Atmospheric Sciences*, *61*(16), 1993–2015. [https://doi.org/10.1175/1520-0469\(2004\)061<1993:TVOMTP>2.0.CO;2](https://doi.org/10.1175/1520-0469(2004)061<1993:TVOMTP>2.0.CO;2)
- Scully, M. E. (2010). Wind modulation of dissolved oxygen in Chesapeake Bay. *Estuaries and Coasts*, *33*, 1164–1175. <https://doi.org/10.1007/s12237-010-9319-9>
- Scully, M. E. (2013). Physical controls on hypoxia in Chesapeake Bay: A numerical modeling study. *Journal of Geophysical Research: Oceans*, *118*, 1239–1256. <https://doi.org/10.1002/jgrc.20138>
- Scully, M. E. (2016a). Mixing of dissolved oxygen in Chesapeake Bay driven by the interaction between wind-driven circulation and estuarine bathymetry. *Journal of Geophysical Research: Oceans*, *121*, 5639–5654. <https://doi.org/10.1002/2016JC011924>
- Scully, M. E. (2016b). The contribution of physical processes to inter-annual variations of hypoxia in Chesapeake Bay: A 30-yr modeling study. *Limnology and Oceanography*, *61*(6), 2243–2260. <https://doi.org/10.1002/lno.10372>
- Shchepetkin, A. F., & McWilliams, J. C. (2005). The regional oceanic modeling system (ROMS): A split-explicit, free-surface, topography-following-coordinate oceanic model. *Ocean Modelling*, *9*(4), 347–404. <https://doi.org/10.1016/j.ocemod.2004.08.002>
- Skamarock, W. C., Klemp, J. B., Dudhia, J., Gill, D. O., Barker, D. M., Wang, W., & Powers, J. G. (2005). A description of the advanced research WRF version 2 (No. NCAR/TN-468+ STR). National Center for Atmospheric Research Boulder Co Mesoscale and Microscale Meteorology Div.
- Slangen, A. B. A., Katsman, C. A., Vermeersen, L. L. A., & Riva, R. E. M. (2012). Towards regional projections of twenty-first century sea-level change based on IPCC SRES scenarios. *Climate Dynamics*, *38*, 1191–1209. <https://doi.org/10.1007/s00382-011-1057-6>
- Stramma, L., Johnson, G. C., Sprintall, J., & Mohrholz, V. (2008). Expanding oxygen-minimum zones in the tropical oceans. *Science*, *320*(5876), 655–658. <https://doi.org/10.1126/science.1153847>

- Taylor, K. E. (2001). Summarizing multiple aspects of model performance in a single diagram. *Journal of Geophysical Research*, *106*(D7), 7183–7192. <https://doi.org/10.1029/2000JD900719>
- Testa, J. M., Brady, D. C., Di Toro, D. M., Boynton, W. R., & Kemp, W. M. (2013). Sediment flux modeling: Nitrogen, phosphorus and silica cycles. *Estuarine, Coastal and Shelf Science*, *131*, 245–263. <https://doi.org/10.1016/j.ecss.2013.06.014>
- Testa, J. M., Li, Y., Lee, Y. J., Li, M., Brady, D. C., Di Toro, D. M., et al. (2014). Quantifying the effects of nutrient loading on dissolved O₂ cycling and hypoxia in Chesapeake Bay using a coupled hydrodynamic–biogeochemical model. *Journal of Marine System*, *139*, 139–158. <https://doi.org/10.1016/j.jmarsys.2014.05.018>
- Testa, J. M., Murphy, R. R., Brady, D. C., & Kemp, W. M. (2018). Nutrient- and climate-induced shifts in the phenology of linked biogeochemical cycles in a temperate estuary. *Frontiers of Marine Science*, *5*, 114. <https://doi.org/10.3389/fmars.2018.00114>
- Wang, P., Linker, L., Wang, H., Bhatt, G., Yactayo, G., Hinson, K., & Tian, R. (2017). Assessing water quality of the Chesapeake Bay by the impact of sea level rise and warming. *IOP Conference Series: Earth and Environmental Science*, *82*, 012001. <https://doi.org/10.1088/1755-1315/82/1/012001>
- Wilson, R. E., Swanson, R. L., & Crowley, H. A. (2008). Perspectives on long-term variations in hypoxic conditions in western Long Island Sound. *Journal of Geophysical Research*, *113*, C12011. <https://doi.org/10.1029/2007JC004693>
- Wood, A. W., Leung, L. R., Sridhar, V., & Lettenmaier, D. P. (2004). Hydrologic implications of dynamical and statistical approaches to downscaling climate model outputs. *Climate Change*, *62*(1-3), 189–216. <https://doi.org/10.1023/B:CLIM.0000013685.99609.9e>
- Xie, X., & Li, M. (2018). Effects of wind straining on estuarine stratification: A combined observational and modeling study. *Journal of Geophysical Research: Oceans*, *123*, 2363–2380. <https://doi.org/10.1002/2017JC013470>
- Xie, X., Li, M., Scully, M., & Boicourt, W. C. (2017). Generation of internal solitary waves by lateral circulation in a stratified estuary. *Journal of Physical Oceanography*, *47*(7), 1789–1797. <https://doi.org/10.1175/JPO-D-16-0240.1>
- Yu, L., Fennel, K., & Laurent, A. (2015). A modeling study of physical controls on hypoxia generation in the northern Gulf of Mexico. *Journal of Geophysical Research: Oceans*, *120*, 5019–5039. <https://doi.org/10.1002/2014JC010634>
- Zervas, C. (2009). Sea level variations of the United States 1854–2006. NOAA Technical Report NOS CO-OPS 053.
- Zhou, Y., Scavia, D., & Michalak, A. M. (2014). Nutrient loading and meteorological conditions explain interannual variability of hypoxia in Chesapeake Bay. *Limnology and Oceanography*, *59*(2), 373–384. <https://doi.org/10.4319/lo.2014.59.2.0373>
- Zillén, L., Conley, D. J., Andrén, T., Andrén, E., & Björck, S. (2008). Past occurrences of hypoxia in the Baltic Sea and the role of climate variability, environmental change and human impact. *Earth-Science Reviews*, *91*, 77–92. <https://doi.org/10.1016/j.earscirev.2008.10.00>